Redox Biology 85 (2025) 103746

Contents lists available at ScienceDirect

Redox Biology

journal homepage: www.elsevier.com/locate/redox

Anemoside B4 alleviates ulcerative colitis by attenuating intestinal oxidative stress and NLRP3 inflammasome via activating aryl hydrocarbon receptor through remodeling the gut microbiome and metabolites

Hao Wu [a,1], Yao-lei Li [b,1], Yu Wang [c,1], Yu-ge Wang [a], Jia-hui Hong [a], Mi-mi Pang [d,*], Pan-miao Liu [a,**], Jian-jun Yang [a,***]

[a] Department of Anesthesiology, Pain and Perioperative Medicine, The First Affiliated Hospital of Zhengzhou University, Zhengzhou, 450000, China
[b] National Institutes for Food and Drug Control, Beijing, 102629, China
[c] Department of Clinical Chinese Pharmacy, School of Chinese Materia Medica, Beijing University of Chinese Medicine, Beijing, 100029, China
[d] Henan Key Laboratory of Chronic Disease Prevention and Therapy & Intelligent Health Management, The First Affiliated Hospital of Zhengzhou University, Zhengzhou, 450000, China

ARTICLE INFO

Keywords:
Ulcerative colitis
Anemoside B4
Aryl hydrocarbon receptor
Gut microbiome
Butyric acid
Oxidative stress

ABSTRACT

Ulcerative colitis (UC) is a chronic, non-specific inflammatory disease of the intestines with a significant increase in global incidence in recent years. Oxidative stress and inflammation are two hallmarks of UC pathogenesis. Anemoside B4 (AB4), a pentacyclic triterpenoid saponin, exhibits significant antioxidant and anti-inflammatory properties and shows potential for preventing UC. Here, an animal model induced by dextran sodium sulfate (DSS) was used to investigate the effect of AB4 on UC. The results demonstrated that AB4 significantly reduces intestinal oxidative stress and inflammation in UC mice, while also protecting intestinal barrier function. Furthermore, AB4 helps restore intestinal microbial balance primarily by modulating the abundance of *Lactobacillus*, which enhances the metabolism of short-chain fatty acids and upregulates the production of butyric acid (BA). Pseudogerm-free mice and fecal microbiota transplantation (FMT) demonstrated that AB4 significantly mitigated UC in a gut microbe-dependent manner. Both AB4 and BA markedly activate the aromatic hydrocarbon receptor (AhR). The intestinal organoid results suggest BA may activate the AhR to inhibit ROS production and activation of NLRP3 inflammasome, thereby protecting intestinal integrity. Administration of AhR antagonists abolished the protective effects, thus confirming the involvement of AhR in the underlying mechanism. Overall, these results indicate that AB4 is an effective agent against UC mainly by activating the AhR through gut microbial short-chain fatty acid metabolites to inhibit intestinal oxidative stress and inflammation.

1. Introduction

Ulcerative colitis (UC) is a chronic, inflammatory disease that primarily affects the submucosa of the colon and rectum. It is the most common form of inflammatory bowel disease (IBD). The clinical symptoms of UC include diarrhea, abdominal pain, blood in the stool, and weight loss [1–3]. The main pathological changes in UC begin as a retrograde process starting from the rectum and can involve the entire colon. This process leads to edema, congestion, erosions, hemorrhages, abscesses, and ulcers in the intestinal mucosa, significantly impacting patients' quality of life and economic well-being [4–6]. UC has a prolonged course, is prone to recurrent episodes, and is challenging to treat, with its incidence rising worldwide in recent years. The development of UC is closely associated with genetic, environmental, and immunological factors, though its exact pathogenesis remains unclear [7–9]. Presently, drugs such as aminosalicylic acid and salazosulfapyridine are used for the treatment of UC. However, these medications can lead to drug tolerance and serious side effects [10–12]. Consequently, identifying and developing new, effective therapies for UC is an urgent clinical problem.

* Corresponding author. The First Affiliated Hospital of Zhengzhou University, East Jian-she Road, Er-qi District, Zhengzhou, 450000, China.
** Corresponding author. The First Affiliated Hospital of Zhengzhou University, East Jian-she Road, Er-qi District, Zhengzhou, 450000, China.
*** Corresponding author. The First Affiliated Hospital of Zhengzhou University, East Jian-she Road, Er-qi District, Zhengzhou, 450000, China.
E-mail addresses: mimi56661@126.com (M.-m. Pang), liupan3374@126.com (P.-m. Liu), yjyangjj@126.com (J.-j. Yang).
[1] These authors contributed equally to this work.

https://doi.org/10.1016/j.redox.2025.103746
Received 21 April 2025; Received in revised form 27 June 2025; Accepted 27 June 2025
Available online 28 June 2025

Recent studies have indicated an imbalance in gut microbiota that is closely associated with UC [13–15]. This imbalance may contribute to disease pathology by altering the composition of gut bacteria, leading to increased levels of pathogenic bacteria, as well as affecting the distribution of metabolites derived from gut microbes [16–20]. Short-chain fatty acids (SCFAs) are important microbial metabolites generated from the bacterial fermentation of dietary fiber and primarily serve as an energy source for colonic cells [21–23]. Current research suggests that SCFAs are essential in the colon and are produced by gut microbes, with their expression levels influencing the processes associated with UC. Healthy gut microbes help regulate the expression of tight junction proteins through SCFAs, thereby maintaining the integrity of the intestinal barrier [24–27].

It is well known that reactive oxygen species (ROS) are primarily produced in the colon, which contains food, microorganisms, and immune cells—these being the main sources of ROS. At high concentrations, ROS can negatively impact colon health, affect microbial diversity, and contribute to disease progression in UC [28–31]. In contrast, SCFAs produced by gut microbes play a protective role against oxidative stress in the colon. They accomplish this by reducing ROS production, decreasing myeloperoxidase (MPO) activity, and enhancing superoxide dismutase (SOD) and catalase (CAT) activity in both the serum and colon [32]. SCFAs also promote glucose uptake, increase fatty acid oxidation, boost oxidative phosphorylation, and support mitochondrial biosynthesis. These actions help maintain the integrity of the intestinal epithelial barrier, foster a tolerogenic intestinal mucosal immune system, and activate the NLRP3 inflammasome, which produces interleukin-1 beta (IL-1β) [33–35].

Additionally, SCFA metabolites have emerged as a promising strategy for treating UC. These metabolites have diverse roles in regulating both the adaptive and innate immune systems, as well as various physiological processes that affect UC, acting as ligands for the aromatic hydrocarbon receptor (AhR) [36,37]. SCFAs can affect immune cells by activating the AhR [38]. This receptor plays a crucial role in T-cell differentiation, antioxidant responses, and NLRP3 inflammasome activation [39–41].

Natural products are a fundamental source of chemical diversity and play a crucial role in drug discovery, prompting us to explore valuable active molecules targeting UC [42–45]. Anemoside B4 (AB4), a pentacyclic triterpenoid saponin, has demonstrated various pharmacological effects, including anti-inflammatory, antioxidant, anti-tumor, antiviral, and immunomodulatory properties [46–50]. Based on these effects, we hypothesized that AB4 might have a therapeutic impact on UC. However, the detailed mechanisms and potential therapeutic targets of AB4 concerning UC remain unclear.

This study aims to evaluate the anti-UC activity about inhibits intestinal oxidative stress and inflammation of AB4 and to investigate its effects on gut microbiota composition and metabolome through 16S rRNA-based microbiota analysis and metabolomics. Fecal microbiota transplantation (FMT) was utilized to confirm that the protective effects of AB4 are modulated in a gut microbiome-dependent manner. Our findings indicated that AB4 significantly enriched gut microbiota-derived SCFA metabolites, which may alleviate UC by directly targeting the AhR. We identified butyric acid as a key mediator of the beneficial effects of AB4 on UC. Additionally, intestinal organoid studies demonstrated that butyric acid can be used to treat UC by activating the AhR signaling pathway. Overall, this research highlights AB4 as a promising drug to inhibit intestinal oxidative stress and inflammation for treating UC and clarifies its mechanism of action.

2. Materials and methods

2.1. Materials

Dextran sulfate sodium (DSS, MW 36–50 kDa) was purchased from MP Biomedicals (Irvine, CA, USA). Anemoside B4 (purity >99 %) was purchased from Macklin Biochemical Co., Ltd. (Shanghai, China). Antibodies to NLRP3 (27458-1-AP) and β-Actin were purchased from Proteintech (Rosemont, IL, USA). The reagents for the detection of MPO, MDA, GSH, SOD, and DCHF-DA were purchased from Solarbio (Beijing, China). Reagent test kits of TNF-α, IL-6, IL-17, IL-1β, ASC, and Caspase-1 were purchased from Jianglai (Shanghai, China). The reagents for the detection of serum creatinine (Cre), serum urea nitrogen (BUN), propionic acid, and butyric acid test kits were purchased from Jiancheng Biological Technology, Co., Ltd (Nanjing, China). The primary antibody against muc-2 was obtained from Abcam (Cambridge, MA, USA). Anti-ZO-1 and anti-Occludin were purchased from Cell Signaling Technology (Danvers, MA, USA). Mouse Intestine Organoid Kits were purchased from Mogengel Biological Technology, Co., Ltd (Xiamen, China). CCK-8 kit (C0041) and DCFH-DA staining solution (S0033S) were purchased from Beyotime Biotechnology (Shanghai, China). AhR test kit was purchased from Renjie Biological Technology, Co., Ltd (RJ17093) (Shanghai, China).

2.2. Animals

Male C57BL/6 mice (6–8 weeks of age, 22 ± 2 g) were purchased from the SPF (Beijing) Biotechnology Co. Ltd (SCXK 2019-0010). All mice were housed in a specific pathogen-free (SPF) environment with a 12 h light/dark cycle, temperature control (22–24 °C), humidity control (50–60 %), and free access to water and food. All animal experiments were conducted by the Guidelines for the Humane Use of Animals published by the National Institutes of Health and approved by the Welfare and Ethics Committee of the Zhengzhou University Laboratory Animal Centre (Approval number: NO. 202206290101).

2.2.1. UC model establishment and treatment

Mice were acclimatized in SPF environment for 7 days, then all mice were randomly divided into 5 groups (12 mice in each group): control group (Con), DSS group (Mod), DSS+5-aminosalicylic acid, as a positive control for alleviating the DSS-induced UC model (5-ASA, 100 mg kg-1), DSS + AB4 low dose group (AB4-L, 50 mg kg-1), DSS + AB4 high dose group (AB4-H, 100 mg kg-1). The mice were fed ad libitum with 3 % DSS (W/V) for 7 days to establish the UC model. Mice in the Con group were fed ad libitum with distilled water. Mice in the Con and Mod groups were fed with sterile water (10 mL kg-1), and the mice in the 5-ASA group were fed with the corresponding drug concentration once a day. The mice in the AB4 group (the optimal dosage range of AB4 was selected based on the results of the preliminary experiments) were given the corresponding drug concentration by rectal administration once a day.

2.2.2. Fecal microbiota transplantation treatment

After a 1-week adaptive feeding period, all mice received antibiotics (Abs: containing 1 g/L neomycin sulfate, 0.5 g/L vancomycin, 1 g/L ampicillin, and 1 g/L metronidazole) in their drinking water for 7 days to generate pseudogerm-free conditions. The donor mice were randomly divided into Con, Mod, and AB4 groups (12 mice in each group). The Con group was fed typically, the Mod and AB4 groups had UC induced by adding 3 % DSS to the drinking water. The Con group mice were dosed with sterile water (10 mL kg-1). The AB4 group was treated with AB4 (100 mg kg-1) by rectal administration once daily. The feces of donor mice were collected daily for 7 days in a laminar flow fume hood under aseptic conditions. Donor mouse feces were collected from each group, and 100 mg of feces was resuspended in 1 ml of sterile saline. The supernatant was collected and used as transplantation material. Fresh graft material was prepared within 10 min before tube feeding on the day of transplantation to prevent changes in bacterial composition. The recipient mice were randomly divided into three groups of fecal transplantation: FT-Con, FT-Mod, and FT-AB4. Recipient mice in FT-Mod and FT-AB4 groups were induced with 3 % DSS in drinking water to induce UC, and recipient mice in FT-Con group were dosed with sterile water.

Fresh fecal graft material from the donor group was administered orally every day for 7 consecutive days.

2.2.3. Short-chain fatty acid metabolites treatment

To verify the role of SCFA metabolites in improving UC damage, the mice were randomly divided into 5 groups (n = 8): control group (Con), DSS group (Mod), DSS+5-aminosalicylic acid positive group (5-ASA, 100 mg kg-1), DSS + sodium propionate group (PA, 150 mM), DSS + sodium butyrate group (BA, 150 mM). After that, mice were fed ad libitum with 3 % DSS (W/V) for 7 d to establish the UC model. Mice in the Con group were fed ad libitum with distilled water. Mice in the Con and Mod groups were dosed with sterile water (10 mL kg-1, ig), and mice in the 5-ASA, PA, and BA groups were dosed with the corresponding drug concentration once a day.

2.2.4. AHR inhibitor treatment

To investigate the pivotal role of AhR in the amelioration of UC by AB4, mice were administered an AhR inhibitor (AHRi), Stemregenin 1. Mice were randomly divided into five groups (8 mice per group) in an SPF environment: control group (Con), DSS group (DSS), DSS + AB4+AHRi (AB4, 100 mg kg-1, Stemregenin 1, 50 mg kg-1), DSS + BA + AHRi (BA, 150 mM, Stemregenin 1, 50 mg kg-1), DSS + AB4 (AB4, 100 mg kg-1, rectal administration). The mice were fed ad libitum with 3 % DSS (W/V) for 7 d to establish the UC model. Mice in the Con group were fed ad libitum with distilled water. Mice in the Con and Mod groups were dosed with sterile water (10 mL kg-1), and mice in the AB4+AHRi, BA + AHRi, and AB4 groups were dosed with the corresponding drug concentration once a day.

At the end of the experiment, all mice were executed by inhalation of isoflurane after the experiment, and a rapid collection of blood samples and colon tissues was performed for subsequent analyses.

2.3. DAI score

DAI was measured according to weight loss, diarrhea, and stool blood. The evaluation criteria of weight loss, diarrhea, and hematochezia were referred to the previously reported [51]. Weight loss (0, none, 1, 1–5 %, 2, 6–10 %, 3, 11–20 %, 4, >20 %), diarrhea (0, normal stools, 1, loose but formed, 2, loose unformed, 3, very loose, 4, severe diarrhea), bleeding in stools (0, negative, 1, weakly positive, 2, positive, 3, markedly positive, 4, rectal bleeding).

2.4. General morphological score

Visual inspection of the colonic mucosa for inflammation and ulceration. The scoring criteria were: no damage to the mucosa (0 points), congestion of the mucosa (1 point), ulceration in less than 25 % of the damaged area (2 points), ulceration in 25 %–50 % of the damaged area (3 points), ulceration in more than 50 % of the damaged area (4 points) [52].

2.5. Histopathological score

The histopathological score was used as the primary criterion for evaluating the degree of inflammation, and the score was as follows 0 points, normal, no inflammatory cell infiltration; 1 point, mild inflammatory cell infiltration without submucosal tissue damage; 2 points, moderate inflammatory cell infiltration and submucosal tissue damage (10–25 % of the extent of the damage); 3 points, marked inflammatory cell infiltration, submucosal tissue damage, and thickening of the colonic wall (25–50 %); 4 points, severe inflammatory cell infiltration, severe colonic tissue damage, and thickening of the colonic wall (>50 % lesion extent) [53].

2.6. Measurement of biochemical indicators in UC mice

Blood samples were centrifuged at 3500 rpm (4 °C) for 15min. Serum was collected, and the TNF-α, IL-1β, IL-6, and IL-17 expression levels were detected according to the kit instructions. The colon tissue was collected, and homogenized AHR, MPO, SOD, MDA, and GSH expression levels were detected according to the kit instructions.

2.7. Immunofluorescence staining

For immunofluorescence analysis of colon tissue, sections were fixed in pre-cooled acetone (15 min) and permeabilized with 3 % Triton X-100. Sections were blocked with 1 % BSA at room temperature (30 min). Sections were washed repeatedly with PBS and incubated overnight at 4 °C with primary antibodies, including ZO-1 (1:250), Occludin (1:250), and muc-2 (1:250). The next day, secondary antibodies were added and incubated for 2 h at room temperature, and the nuclei were stained with 4′,6-diamidino-2-phenylindole (DAPI) reagent. Fluorescence microscopy was used for photographic imaging.

2.8. Reactive oxygen species (ROS) detection

Total ROS was detected by DCFH-DA staining. Single-cell suspensions were prepared from fresh colon tissue samples by enzymatic digestion (collagenase I). The cells were incubated with DCFH-DA staining solution (10 mol/L) at 37 °C for 20 min, centrifuged for 10 min (1000 g). Subsequently, the cells were washed with PBS three times and centrifuged. Finally, the difference of average fluorescence intensity was compared by flow cytometry.

2.9. Immunohistochemistry

The sections were dewaxed in xylene and graded alcohol, then washed in cold PBS. All subsequent steps were performed under humidified conditions. Enzymatic antigen repair was conducted at 37 °C for 30 min to restore the antigen. The slices were washed three times with PBS, with each wash lasting 3 min. Non-specific antigens were blocked using goat serum at 25 °C for 30 min. Next, the slices were incubated overnight at 4 °C with anti-caspase-1 antibodies (1:100, 22915-1-AP; Proteintech Group) and anti-GSDMD antibodies (1:100; ab239377, Abcam). After that, they were treated with biotin-labeled goat anti-mouse/rabbit IgG polymer for 30 min. Streptavidin/horseradish peroxidase was then incubated at 25 °C for 30 min, followed by washing with PBS. The sections were stained with diaminobenzidine and subsequently re-stained with hematoxylin for 5 min. After dehydration, the sections were sealed. Images of the sections were captured using an optical microscope. Positive staining was indicated by brown color, and Image J software was used to analyze the optical density value of the positively stained area, which represented the expression levels of Caspase-1 and GSDMD.

2.10. Western blot

Remove colon tissue samples for tissue homogenization and cell lysis. The samples were rinsed three times with PBS, and protein samples were separated by cell lysis. Protein concentration was detected using the BCA Protein Assay Kit (Beyotime Biotech Inc, China). Protein samples were separated and electrophoresed on sodium dodecyl sulfate-polyacrylamide gel electrophoresis (SDS-PAGE) gels (70 V, 120 min). Protein bands were transferred onto polyvinylidene difluoride (PVDF) membranes (Bio-Rad, Hercules, CA, USA). The PVDF membranes were incubated overnight at 4 °C with diluted primary antibody. Then, the protein signals were measured with an enhanced chemiluminescence visualization (ECL) system (Pierce Biotechnology) after 2 h of incubation with horseradish peroxidase (HRP)-labeled secondary antibody. The intensity of the protein bands was analyzed using Image Lab

analysis software (Bio-Rad).

2.11. 16S rRNA sequencing

The total genomic DNA of the microbial community was extracted from each group of mouse fecal samples according to the instructions of the PF Mag-Bind Stool DNA Kit (Omega Bio-tek, Georgia, U.S.). The integrity of the extracted genomic DNA was tested by agarose gel electrophoresis at 1 %, and the concentration and purity of DNA were determined by NanoDrop2000 (Thermo Scientific, U.S.). The upstream primer 338F (5'-ACTCCTACGGGGAGGCAGCAG-3') and the downstream primer 806R (5'-GGACTACHVGGGGTWTCTAAT-3'), which carry Barcode sequences, were used to analyze the 16S rRNA. ') for PCR amplification of the V3–V4 variable region of the 16S rRNA gene. The purified PCR products were library-constructed using the NEXTFLEX Rapid DNA-Seq Kit (Bioo Scientific, Austin, Texas, USA) and sequenced using Illumina's PE300/PE250 platforms (Shanghai Meiji Bio-medical Technology Co., Ltd.).

2.12. Untargeted metabolomics

Metabolite extraction was performed by taking 50 mg of fecal sample in a 2 mL centrifuge tube and adding a 6 mm diameter grinding bead. 400 μL of extraction solution (methanol: water = 4:1 (v:v)) containing 0.02 mg/mL of internal standard (L-2-chlorophenylalanine) was used for the extraction of metabolites. The sample solution was ground in a frozen tissue grinder for 6 min (−10 °C, 50 Hz), followed by cryogenic extraction for 30 min (5 °C, 40 kHz). The samples were allowed to stand at −20 °C for 30 min, centrifuged for 15 min (4 °C, 13000 g), and the supernatant was pipetted into an injection vial with an internal cannula for analysis. The sample was separated on a HSS T3 column (100 mm × 2.1 mm i.d., 1.8 μm) and detected by mass spectrometry. Mobile phase A was 95 % water +5 % acetonitrile (containing 0.1 % formic acid), and mobile phase B was 47.5 % acetonitrile + 47.5 % isopropanol + 5 % water (containing 0.1 % formic acid). Mass spectrometry conditions: The sample mass spectrometry signal acquisition was performed in positive and negative ion scanning modes, with a mass scanning range *m/z* of 70–1050. ion spray voltage, positive ion voltage 3500 V, negative ion voltage 2800 V, sheath gas 40 psi, auxiliary heated gas 10 psi, ion source heating temperature 400 °C, 20-40-60 V cyclic collision energy, MS1 resolution: 70,000 and MS2 resolution: 17500.

2.13. Crypt isolation and intestinal organoid culture

After the euthanasia of mice, colonic tissues were removed under aseptic conditions and washed in pre-cooled DPBS to remove the outer layer of the intestinal membrane and surrounding fatty tissue. The intestine was opened longitudinally and rinsed with pre-cooled DPBS. The contents of the intestinal lumen and villous structures were scraped off with a slide. Cut the cleaned bowel into 3 mm pieces of tissue and incubate in EDTA (5 mmol/L) at 4 °C for 30 min. DPBS was added and shaken appropriately to separate the crypts from the basal layer, and the suspension was filtered through a 70 μm cell filter, repeating this cycle three times. The supernatant was centrifuged (300 g, 4 °C, 5 min) to obtain crypts, and an appropriate amount of crypt suspension was aspirated to visualize the crypt morphology through a microscope and counted. The crypts were suspended in pre-cooled DPBS and centrifuged (300 g, 4 °C, 5 min). The crypt spheres were resuspended in cold organoid medium and matrix gel (ratio = 1:1), and the intestinal organoids were further induced on 24-well plates [54].

2.14. Statistical analysis

Statistical analyses were performed using SPSS version 18.0 (Chicago, IL, USA) and plotted using GraphPad Prism software (version 8.0.0, San Diego, CA, USA). All data are expressed as mean ± standard error of the mean (S.E.M). Comparisons between groups were made using one-way analysis of variance (ANOVA) with post-hoc Tukey's test or Student t-test where appropriate.

3. Results

3.1. AB4 attenuates DSS-induced UC in mice

To investigate the therapeutic effect of AB4 on UC, C57BL/6 mice were induced an acute UC mode with 3 % DSS for seven days, which had clinical signs similar to those of UC patients, including weight loss, diarrhea, and bloody stools (Fig. 1A). Mice in the Mod group showed significant weight loss, reduced food and water intake on day 3, severe diarrhea and blood in the stools from day 4 onwards, and reduced DAI scores until the end of the experiment. Colitis mice given AB4 significantly inhibited weight loss, restored food and water intake, and reduced diarrhea, bloody stools, and DAI scores in a dose-dependent manner compared to mice in the Mod group (Fig. 1B–E).

A shorter colon length is an essential visual observation that reflects intestinal damage. After examining the colons of each group of mice, it was found that mice exposed to DSS could significantly shorten the length of the colon. In contrast, colitis mice treated with AB4 significantly prevented DSS-induced colon shortening (Fig. 1 FG). The thickness and general morphology of the colon were further scored. The results showed AB4 treatment significantly attenuated DSS-induced colonic injury in mice and reduced general morphological score (Fig. 1 HI).

H&E staining and analysis of the pathology of the colonic tissues showed that the colonic tissues of mice in the Mod group exhibited pathological damage, including significant loss of cupped cells and epithelial cells, massive inflammatory cell infiltration, and extensively damaged crypt structures. In contrast, treatment with AB4 significantly attenuated the pathological damage of the colonic tissues, reduced inflammatory cell infiltration, restored the crypt structures, and reduced the histopathological scores in a dose-dependent manner (Fig. 1 JK). These results suggest that AB4 attenuated DSS-induced colitis in mice and is a promising agent for treating UC.

3.2. AB4 inhibits inflammation and prevents intestinal barrier dysfunction in UC mice

Mucosal inflammatory infiltration and barrier disruption are major pathologic features of UC, both in DSS-induced animal models and in UC patients. We investigated whether AB4 could attenuate DSS-induced intestinal mucosal inflammation and remodel the intestinal barrier in UC mice. We examined the critical pro-inflammatory factors TNF-α, IL-6, IL-17, and IL-1β in the serum and colon tissues of mice in each group (Fig. 2A–D). The results showed that the pro-inflammatory factors in serum and colonic tissues of mice in the Mod group appeared significantly elevated compared with those in the Con group ($P < 0.001$), suggesting that inflammatory responses were observed in DSS-induced UC mice in vivo. After AB4 treatment, the pro-inflammatory factors in both serum and colonic tissues of mice within the AB4 L and AB4 H groups showed a significant decrease ($P < 0.01$ or $P < 0.001$), suggesting that AB4 has an inhibitory effect on the inflammation induced by DSS in UC mice. In addition, the AB4 H group exhibited superior anti-inflammatory activity than 5-ASA (TNF-α, IL-6 and IL-17), and there was a significant difference statistically ($P < 0.05$ or $P < 0.01$).

Immunofluorescence analysis showed that mice exposed to DSS significantly reduced the expression of ZO-1 and Occludin proteins. Notably, AB4 treatment of UC mice significantly increased the expression of ZO-1 and Occludin proteins in the inner layer of the columnar epithelium of colonic tissue. In addition, a significant increase in mucin-2 (Muc-2) expression was observed in UC mice treated with AB4. These results suggest that AB4 inhibits DSS-induced intestinal mucosal inflammation and protects intestinal barrier function in UC mice (Fig. 2

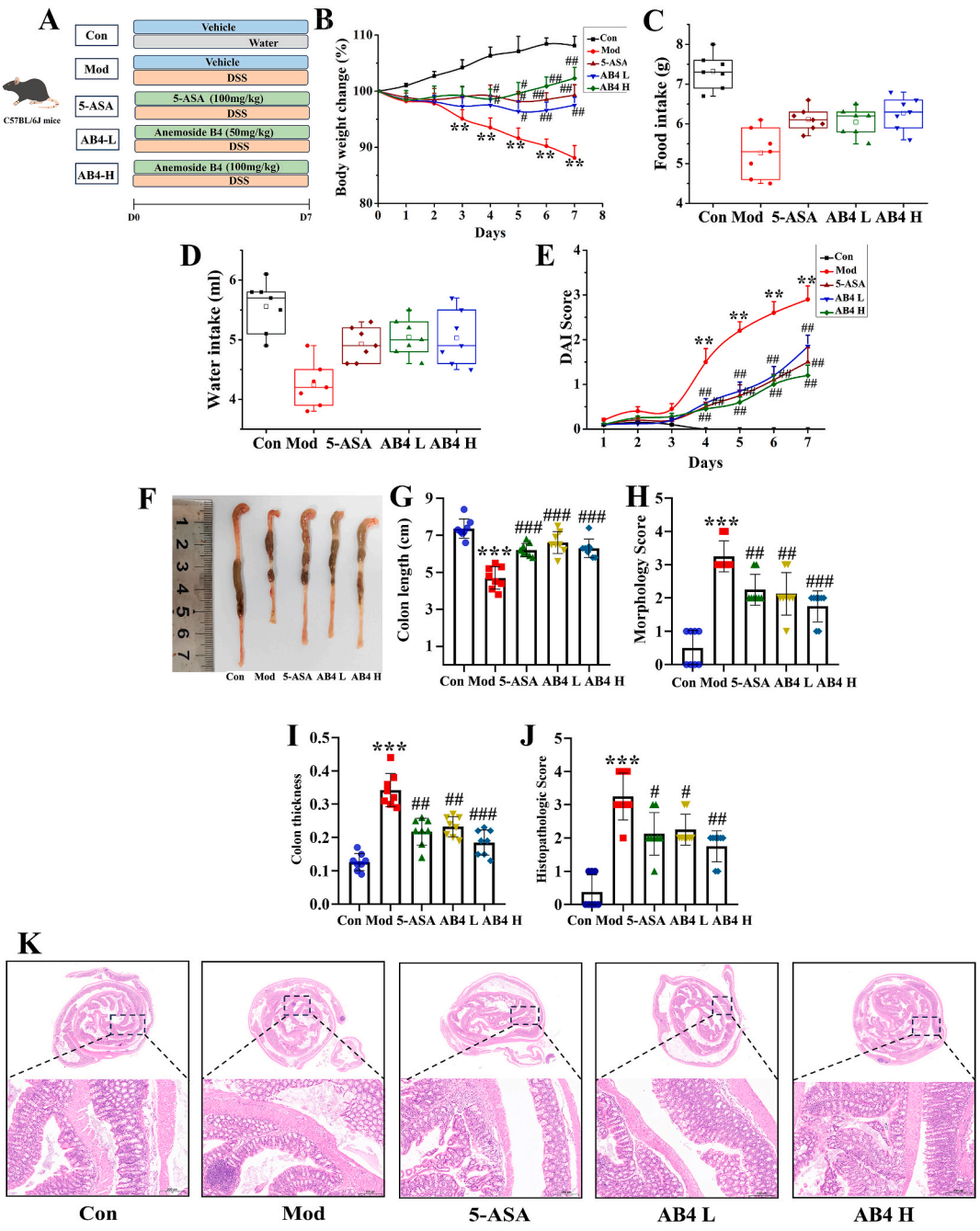

Fig. 1. AB4 alleviates DSS-induced mice colitis. (A) The flowchart of the part in vivo experiments. (B) The body weight of mice in each group. (C) The food intake. (D) The water intake. (E) DAI score. (F) Observation of colonic appearance in mice. (G) Colon length. (H) Morphology score. (I) Colon thickness. (J) Histopathological score. (K) Representative H&E images for colon tissues. Data are expressed as mean ± SEM for 8 mice in each group. $^{*}P < 0.05$, $^{**}P < 0.01$ and $^{***}P < 0.001$ versus Con group, $^{\#}P < 0.05$, $^{\#\#}P < 0.01$ and $^{\#\#\#}P < 0.001$ versus Mod group.

EF).

3.3. Effects of AB4 on gut microbial diversity in UC mice

Gut microbial diversity was determined to study the changes in gut microbes after AB4 (AB4 H, 100 mg kg-1) treatment. Species profiles of OTU (Operational Taxonomic Unit) number sorting rank, Pan, and Core were first analyzed for each group of samples, which indicated that the number of gut microbial species and sequencing sample size of each group was sufficient to support further analysis (Fig. 3A–C). The samples were further analyzed for alpha diversity, including the Sobs index, Shannon index, Chao index, and Ace index, representing the number of samples, sample diversity, sample homogeneity, and sample richness. The results showed that the alpha diversity of gut microorganisms could be significantly increased after AB4 treatment (Fig. 3D–G). The β-diversity was further analyzed by PCA, PcoA, NMDS, and NCM, which indicated that the gut microbial composition of mice in the Con and AB4 groups was significantly different from that of the Mod group. The sample points were closer to each other in the Con and AB4 groups than in the Mod group, indicating that the species composition of the samples in the two groups was more similar. The Neutral Community Model (NCM) was used for the analysis. The results suggested that microbial community construction in each group in this study was more susceptible to deterministic processes and less to stochastic processes

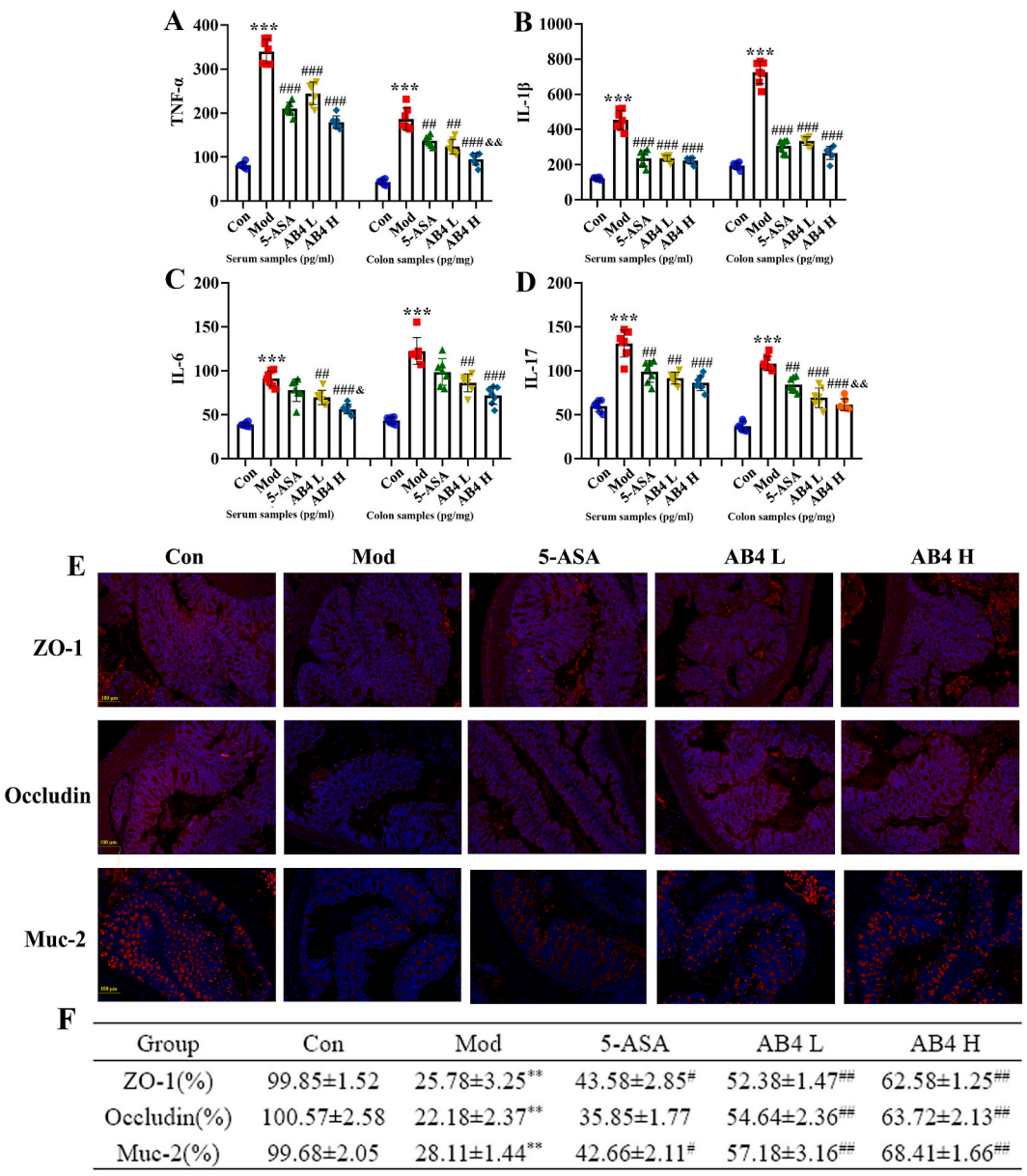

F

Group	Con	Mod	5-ASA	AB4 L	AB4 H
ZO-1(%)	99.85±1.52	25.78±3.25**	43.58±2.85#	52.38±1.47##	62.58±1.25##
Occludin(%)	100.57±2.58	22.18±2.37**	35.85±1.77	54.64±2.36##	63.72±2.13##
Muc-2(%)	99.68±2.05	28.11±1.44**	42.66±2.11#	57.18±3.16##	68.41±1.66##

Fig. 2. AB4 suppressed inflammation and protected against intestinal barrier dysfunction to attenuate colitis in mice. (A–D) Inflammatory cytokines (TNF-α, IL-1β, IL-6, and IL-17) levels in serum and colonic tissues (n = 6). (E–F) Representative immunofluorescence images and the fluorescence intensities of ZO-1, Occludin, and Muc-2 in colonic tissues (n = 3). $^{***}P < 0.001$ versus Con group, $^{\#\#}P < 0.01$ and $^{\#\#\#}P < 0.001$ versus Mod group, $^{\&}P < 0.05$ and $^{\&\&}P < 0.01$ versus 5-ASA group.

(Fig. 3H–K).

Partial Least Squares Discriminant Analysis (PLS-DA) could separate the Con and Mod groups. Despite differences in the composition of the gut microbiota between the Con and AB4 groups, gut microbiota in the AB4 group was more similar to the gut microbiota in the Con group compared to baseline samples in the Mod group (Fig. 3 L). The gut microbial dysbiosis index (MDI) is an index that determines the degree of microbial ecological dysbiosis, and a more significant value indicates a greater degree of dysbiosis. The results suggested that AB4 treatment significantly adjusted the DSS-induced gut dysbiosis (Fig. 3 M). Finally, the clustering of the samples in each group was shown by sample hierarchical clustering, and the OTU-based sample hierarchical clustering tree showed significant differences among the three groups, with the AB4-treated samples clustering separately from the DSS group and closer to the Con group (Fig. 3 N). In conclusion, this part of the results suggests that AB4 treatment significantly restored the gut microbial disruption caused by exposure to DSS in mice, and it may achieve therapeutic effects in UC mice by restoring the diversity of gut microbes.

3.4. *Effect of AB4 on the gut microbial composition in DSS-induced UC mice*

Further in-depth analysis of the alterations in the gut microbiology of mice was performed. First, the number of shared and unique species in multiple groups of samples was counted, which can be used to identify unique species in disease groups and help find biomarkers. After analyzing the samples through Venn diagrams, it was found that there were unique or shared gut microorganisms among the groups of samples (Fig. 4 A). At the phylum level, community abundance analysis showed the Mod group increased the abundance of *Bacteroidota* and *Verrucomicrobiota* and decreased the abundance of *Firmicutes*, *Patescibacteria*, and *Actinobacteriota* and that AB4 treatment reversed the effect of exposure to DSS on these species (Fig. 4 B). We also examined the abundance of gut microbes at the genus level, from which we could

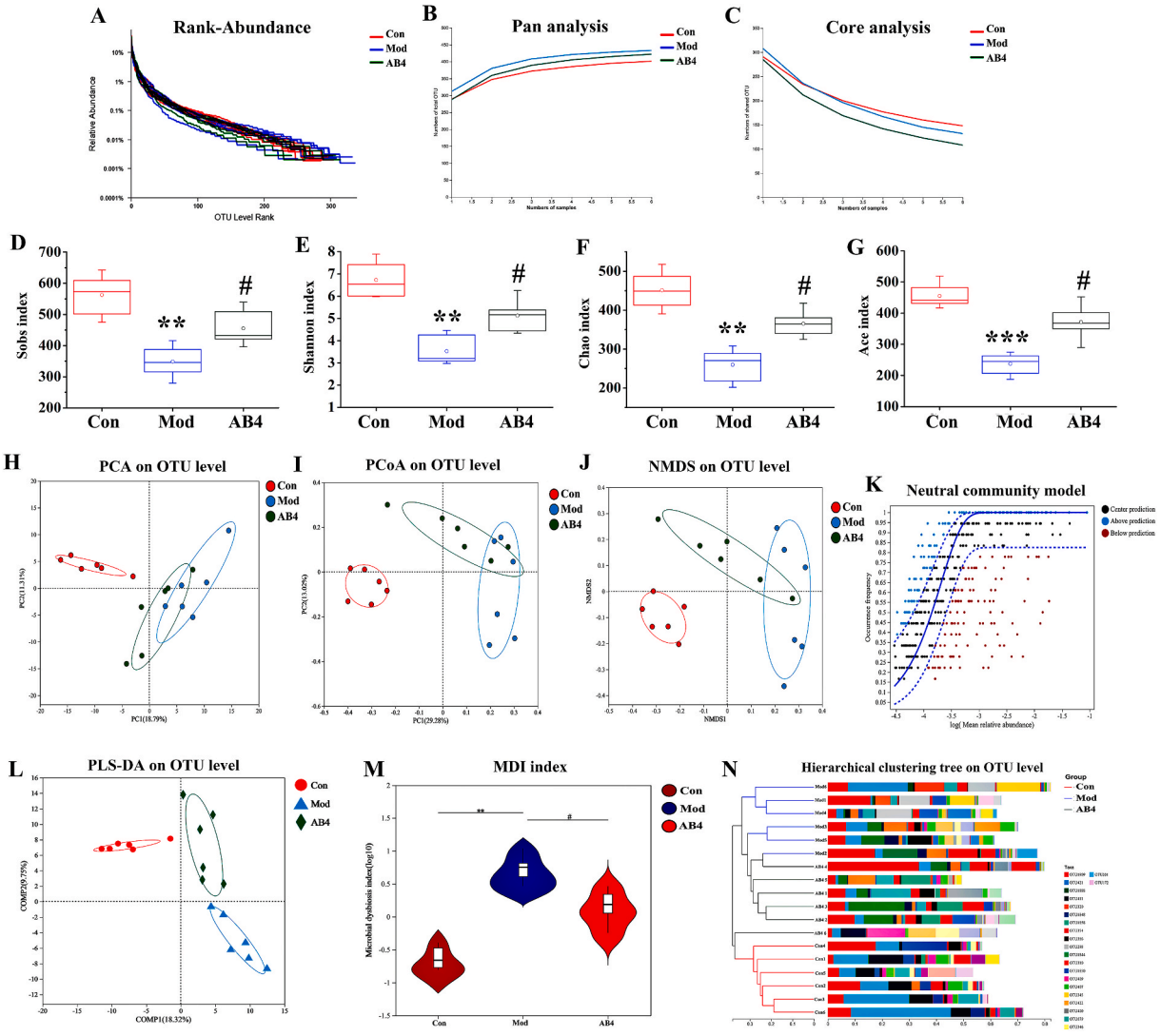

Fig. 3. AB4 improved UC mice by restoring gut microbial diversity. (A) OUT rank. (B) Pan analysis. (C) Core analysis. (D) Sobs index. (E) Shannon index. (F) Chao index. (G) Ace index. (H) PCA analysis. (I) PcoA analysis. (J) NMDS analysis. (K) NCM analysis. (L) PLS-DA analysis. (M) Microbial dysbiosis index. (N) Hierarchical clustering. Data are expressed as mean ± SEM for 6 mice in each group. $^{**}P < 0.01$ and $^{***}P < 0.001$ versus Con group, $^{\#}P < 0.05$ versus Mod group.

observe differences in dominant species between the three groups, with *Muribaculaceae* dominating in the Mod group and *Lactobacillus* dominating in the Con and AB4 group (Fig. 4C).

The circle plot visualizes the correspondence between species and samples, which helps to understand the proportion of species distribution in each group of samples. It also shows the microorganisms and their relative abundance in each group of samples, with relative abundance <0.01 uniformly categorized as others. The results suggest that at the phylum level, there was a higher abundance of *Firmicutes*, *Bacteroidota*, and *Patescibacteria*, while a higher abundance at the genus level was *Muribaculaceae* and *Lactobacillus* (Fig. 4 DE). The Lefse multilevel species difference discriminant analysis tested the difference of differentiated species at multiple levels. It measured the size of the effect of species on the impact of the difference using the LDA value. Only the LDA value of >3.5 is shown. Different colored nodes indicate microbial taxa that are significantly enriched in the corresponding group and significantly affect intergroup differences, identifying characteristic taxa with significant differences in abundance (Fig. 4F–H). The heat map clearly shows the relative abundance of different microorganisms in each group of mice (Fig. 4 G).

Finally, PICRUSt2 functional prediction was used to predict the functional information of microbial communities in each group of samples. The metabolic pathways in the disease process were further predicted by functional composition and abundance (KEGG), which showed that the relevant pathways were focused on *Response to oxidative stress*, *Oxidation-reduction process*, *Oxidative phosphorylation*, *Oxidoreductase activity*, etc., suggesting that the alteration of flora is closely related to redox-related pathways (Fig. 4 I). Thus, the above results suggest that AB4 improved the gut microbial composition in DSS mice, which may contribute to the alleviation of intestinal inflammation and protection of the intestinal barrier.

3.5. *Effect of AB4 on gut microbial metabolites in DSS-induced UC mice*

It is known that the bioavailability of saponins is low, and most dietary saponins exert their function through microbial metabolites fermented by gut microorganisms.

Therefore, liquid chromatography-mass spectrometry (MS) analysis was used to observe the changes in microbial metabolites in the feces after AB4 treatment. PCA analysis can provide a preliminary understanding of the overall metabolic differences between the samples in each group and the magnitude of variability between samples within groups. The results showed that the QC samples were well grouped, indicating good bioanalysis and data quality. This suggests that the

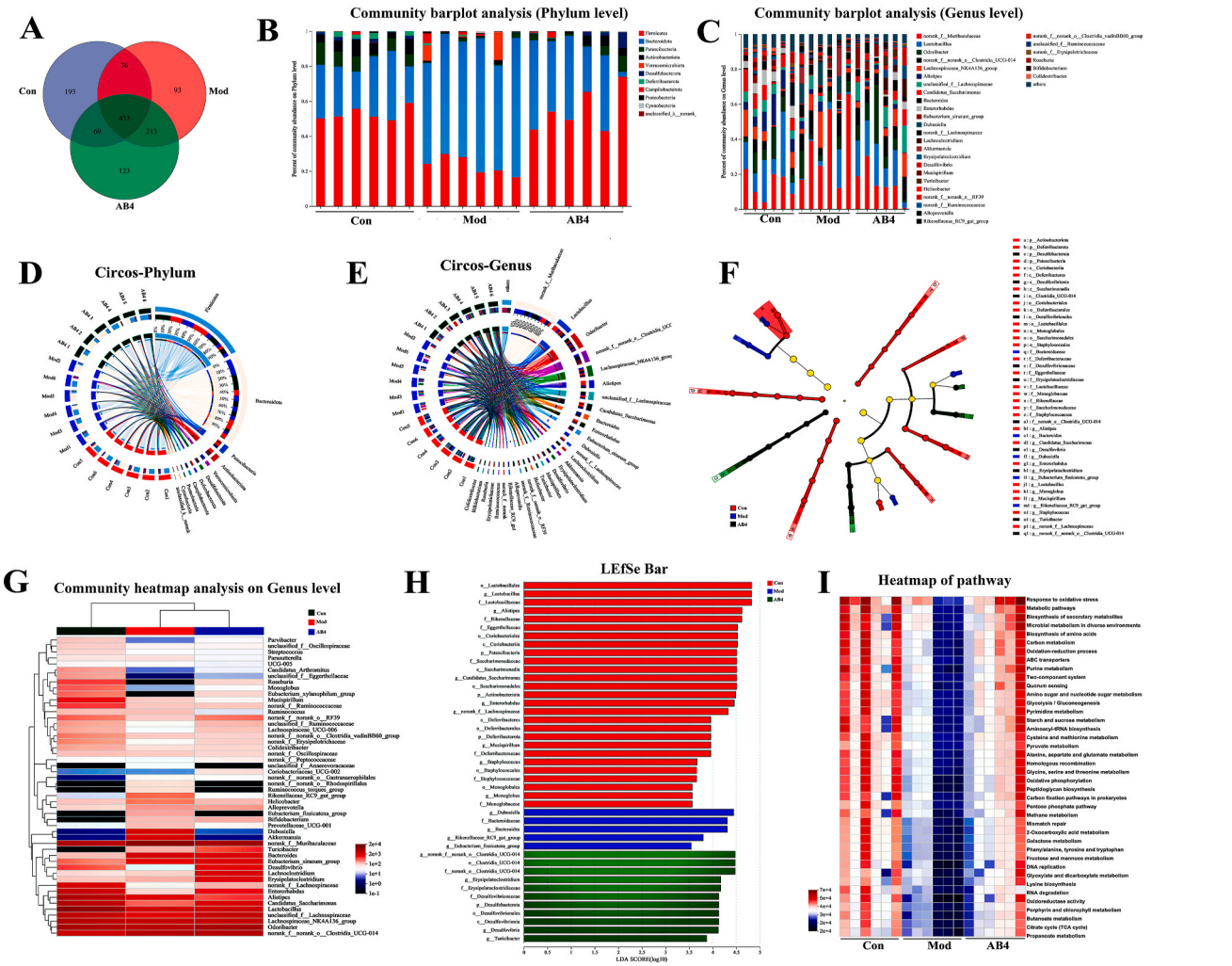

Fig. 4. AB4 improved gut microbial composition in UC mice. (A) Venn diagram. (B) Community abundance analysis at the phylum level. (C) Community abundance analysis at the genus level. (D) Circos plots analysis at the phylum level. (E) Circos plots analysis at the genus level. (F) LEfSe multilevel species level tree. (G) Heat map. (H) LDA discriminant histogram. (I) PICRUSt2 functional prediction.

separation between the groups was due to the different variables rather than differences in the analytical process. In contrast, all three groups of samples could be separated by PCA analysis under positive and negative ions (Fig. 5 AB). Partial least squares discriminant analysis showed that the gut metabolic profiles of mice treated with AB4 significantly differed from those of the Mod group under positive and negative ion analysis (Fig. 5C–H).

Volcano plots showing changes in the number of metabolites showed that 153 were up-regulated and 497 were down-regulated when the Con group was compared with the Mod group. 96 metabolites were up-regulated, and 443 metabolites were down-regulated when the Mod group was compared with the AB4 group, 56 metabolites were up-regulated, and 139 metabolites were down-regulated when the Con group was compared with the AB4 group (Fig. 5I–K). These results indicate that mice treated with AB4 significantly altered the composition of metabolites in the feces of DSS mice.

Further specific analyses of fecal metabolite composition in each group of mice were performed. Firstly, the differential metabolites that were common or specific to the two groups were analyzed for comparison, and the Venn diagrams showed that a total of 73 identical metabolites were altered after AB4 treatment (Fig. 6A). The expression pattern of metabolites in each differential group and the P value of metabolites in VIP and unidimensional statistics of multivariate statistical analysis was demonstrated by VIP bar charts to visualize the importance of differential metabolites and the trend change of expression. The results suggested that short-chain fatty acids (SCFAs) occupied an essential position in analyzing differential metabolites, of which propionic acid and butyric acid had significantly lower expression in the Mod group, and the expression after AB4 treatment was elevated considerably (Fig. 6 BC).

The differentially expressed metabolites were clustered and analyzed to observe the trends of differential metabolite changes in different groups, the results of which similarly suggested that butyric acid was the critical differential metabolite in the intestines of AB4-treated DSS-induced UC mice (Fig. 6 D). The identified metabolites were then analyzed by KEGG pathway classification for enrichment analysis and functional analysis. Scfas were found to be the pathway with the highest enrichment rate and also occupied a crucial position in metabolite functional analysis, suggesting that the short-chain fatty acid pathway may be a critical metabolic pathway in AB4-treated UC mice (Fig. 6E–H).

3.6. AB4 inhibits intestinal oxidative stress and NLRP3 inflammasome activation in UC mice

The results of gut microbial metabolites suggest that SCFAs play a crucial role in the AB4 treatment of UC mice. Therefore, we first clarified the expression level of SCFAs in the colon tissues of the groups, and the

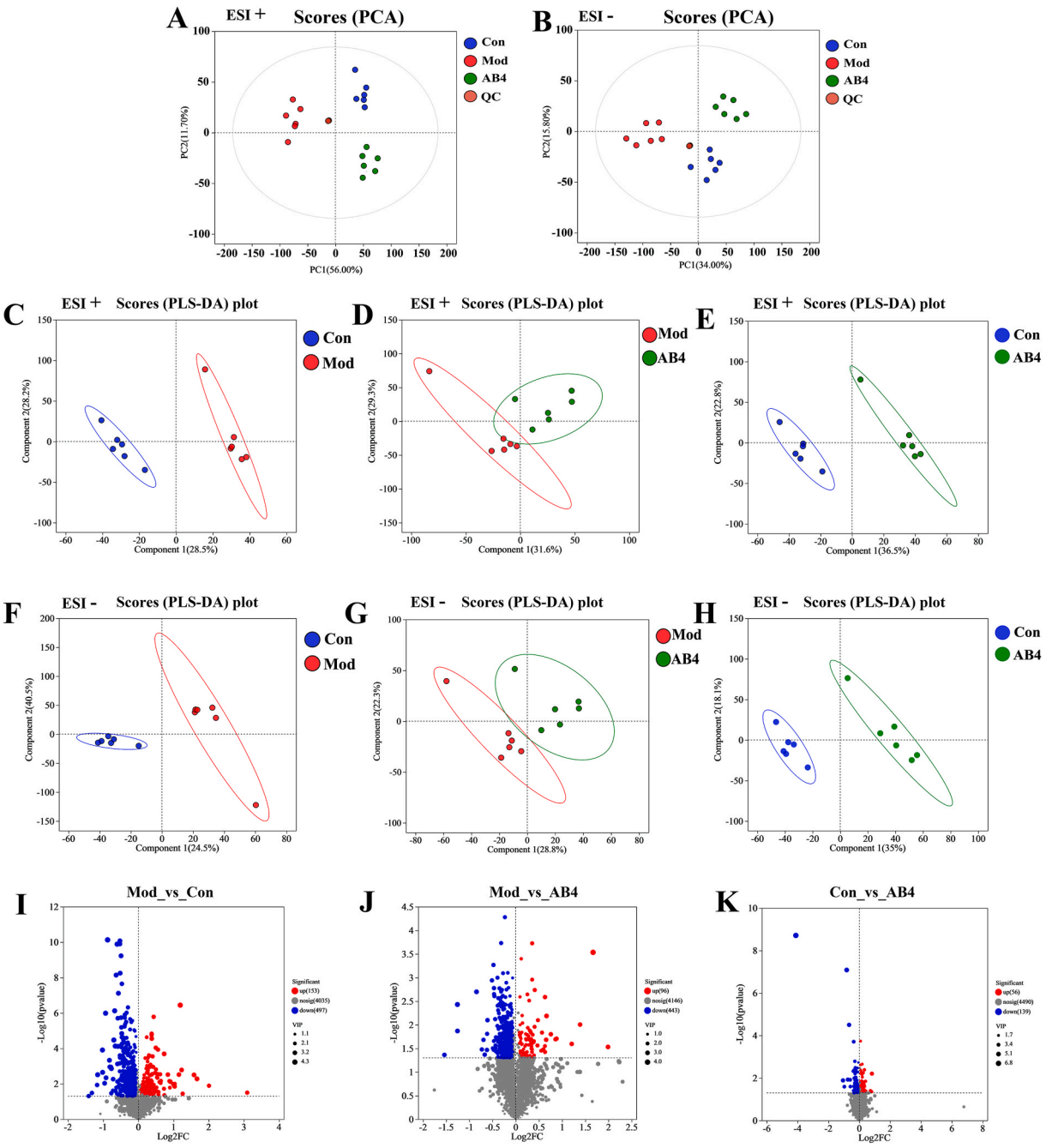

Fig. 5. Effect of AB4 on comparative analysis of gut microbial metabolites in UC mice. (A–B) PCA analysis under positive and negative ions. (C–E) PLSDA analysis under positive ions. (F–H) PLSDA analysis under negative ions. (I–K) Volcano plots.

results showed that the expression of propionic acid and butyric acid was significantly reduced in the Mod group. In contrast, AB4 treatment significantly increased the expression level of SCFAs in the intestine (Fig. 7 AB). SCFAs contribute to maintaining colonic homeostasis, and their elevated expression effectively reduces ROS production and inhibits the activation of NLRP3 inflammasome to produce IL-1β, thereby ameliorating colonic inflammation in UC mice.

In this study, the production of ROS and the expression levels of oxidative stress-related indexes in the colonic tissue samples were further examined. The results showed that the production of ROS in the colonic tissues of the mice in the Mod group were significantly higher compared with those of the Con group ($P < 0.001$), suggesting that oxidative stress occurred in the mice in the Mod group, which facilitated the generation of ROS. After AB4 treatment, the ROS expression level in the colonic tissues of mice in the AB4 group was significantly lower than that in the Mod group ($P < 0.05$), suggesting that AB4 could inhibit DSS-induced ROS generation in colonic tissues of mice (Fig. 7 CD). The contents of MPO, SOD, MDA, and GSH in the colonic tissues of mice were detected. Compared with the Con group, MPO and MDA expression levels in the Mod group were significantly higher ($P < 0.001$). The contents of SOD and GSH were significantly lower ($P < 0.001$). Compared with the Mod group, the contents of MPO and MDA in the colonic tissues of the AB4 group were significantly lower ($P < 0.05$ or $P < 0.01$ or $P < 0.001$). The contents of SOD and GSH were significantly higher ($P < 0.01$ or $P < 0.001$) (Fig. 7E–H). This part of the results suggested that AB4 could effectively inhibit the DSS-induced triggered colonic oxidative stress.

Secondly, The expression levels of NLRP3, ASC, Caspase-1, and IL-1β

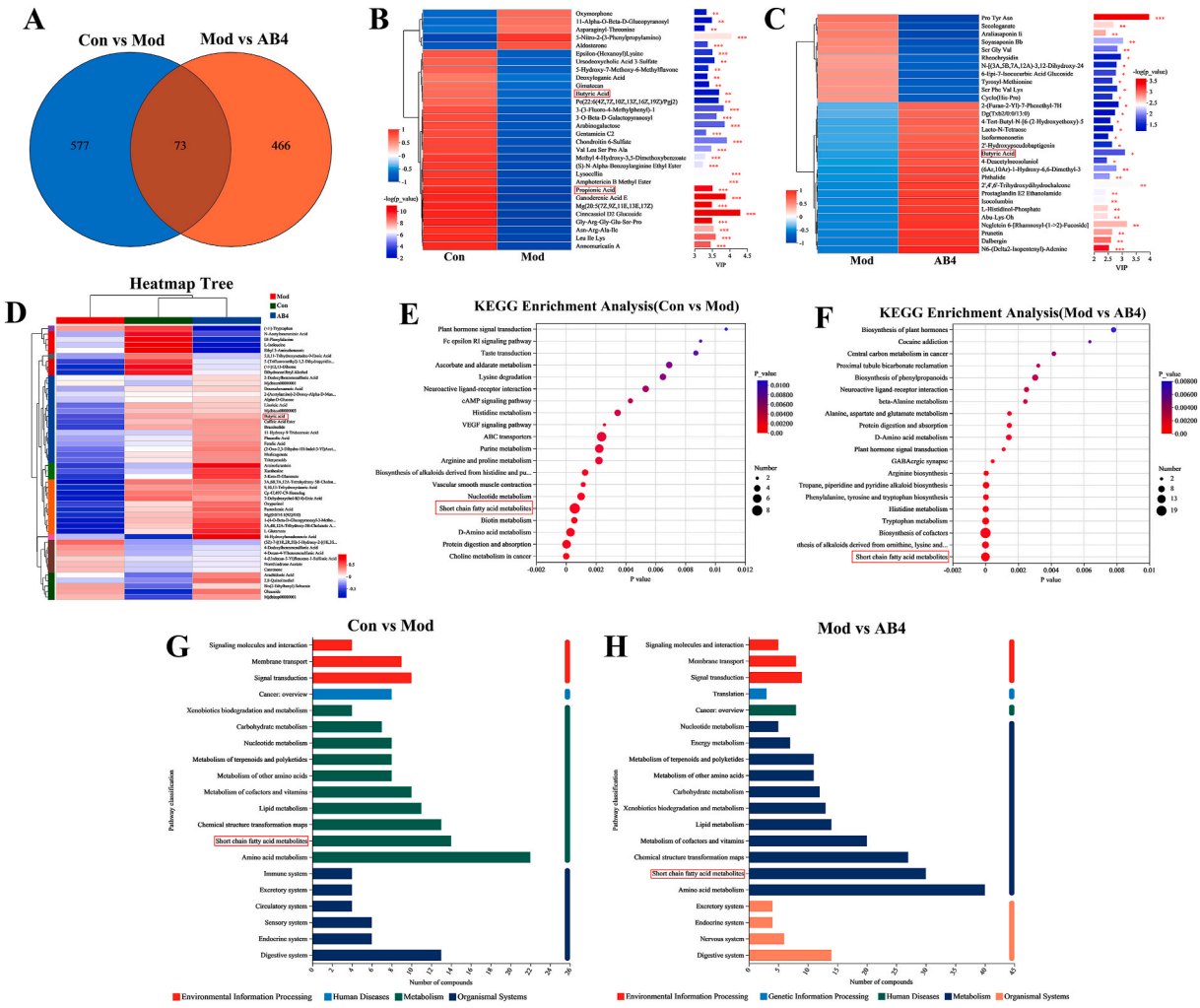

Fig. 6. Effect of AB4 on gut microbial metabolites in DSS-induced UC mice. (A) Venn diagram. (B–C) VIP bar charts. (D) Differential metabolite cluster analysis. (E–F) KEGG enrichment analysis. (G-H)KEGG functional analysis.

were detected in the colonic tissues of mice in each group to clarify the effect of AB4 on NLRP3 inflammasome in UC mice. The results revealed that the expression levels of NLRP3 in the colonic tissues of mice in the Mod group were significantly higher than those in the Con group ($P < 0.001$). In contrast, the expression levels of NLRP3 in mice in the AB4 group were substantially lower than those in the Mod group after treatment ($P < 0.01$ or $P < 0.001$) (Fig. 7 IJ). Moreover, the expression levels of ASC, Caspase-1, and IL-1β in the colonic tissues of mice in the Mod group were significantly higher than those in the Con group ($P < 0.001$). The expression levels of ASC, Caspase-1, and IL-1β in the colonic tissues of both the AB4 H and AB4 L groups were all significantly lower compared with those in the Mod group ($P < 0.05$ or $P < 0.01$ or $P < 0.001$) (Fig. 7K–M). This suggests that NLRP3 inflammasomes are activated during the development of UC, which further promotes the inflammatory response in vivo. In contrast, AB4 treatment can effectively inhibit NLRP3 inflammasomes in UC mice, exerting an anti-inflammatory effect in treating UC.

3.7. AB4 attenuates UC in a gut microbiota short-chain fatty acid metabolites-dependent manner and activating AHR

To verify whether gut microbial mediated the protective effect of AB4 on UC mice, we constructed a germfree colitis mouse model by administering antibiotics to mice prior to DSS treatment. And we transplanted the gut microbiota of AB4-treated DSS mice into recipient Mod mice by daily gavage (Fig. 8 A). Compared to the FT-Mod group, mice in the FT-AB4 group exhibited significantly reduced UC-related symptoms, including recovery of body weight, increased food intake and water intake, and reduced DAI score (Fig. 8B–E). After analyzing the colons of mice in each group 7 days after the experiment, it was found that mice in the FT-Mod group could significantly shorten the length of their colons. In contrast, mice receiving AB4 cecal transplants significantly prevented DSS-induced shortening of their colons (Fig. 8 F). The thickness and general morphology of the colon were further scored. The results showed that the thickness and morphological scores of the colon of mice in the FT-Mod group were significantly higher than those of the FT-Con group ($P < 0.001$) and that mice receiving AB4 fecal transplants significantly attenuated DSS-induced colonic injury (Fig. 8G–I). The cytokines TNF-α, IL-1β, IL-6, and IL-17 were examined in serum and colonic tissues of mice in each group, and the results showed after receiving AB4 fecal transplantation, the pro-inflammatory factors in serum and colonic tissues of mice in the FT-AB4 group appeared to be significantly reduced, suggesting that the anti-inflammatory effect exerted by AB4 on UC mice may be mediated by gut microbiota metabolites (Fig. 8J–M).

Further intestinal HE and immunofluorescence staining were performed on each group of mice to observe pathological changes and effects on the intestinal barrier. The results showed that AB4 fecal transplantation could attenuate the effects of inflammatory infiltration in colonic tissues and restore villi and crypt structures, reduce tissue

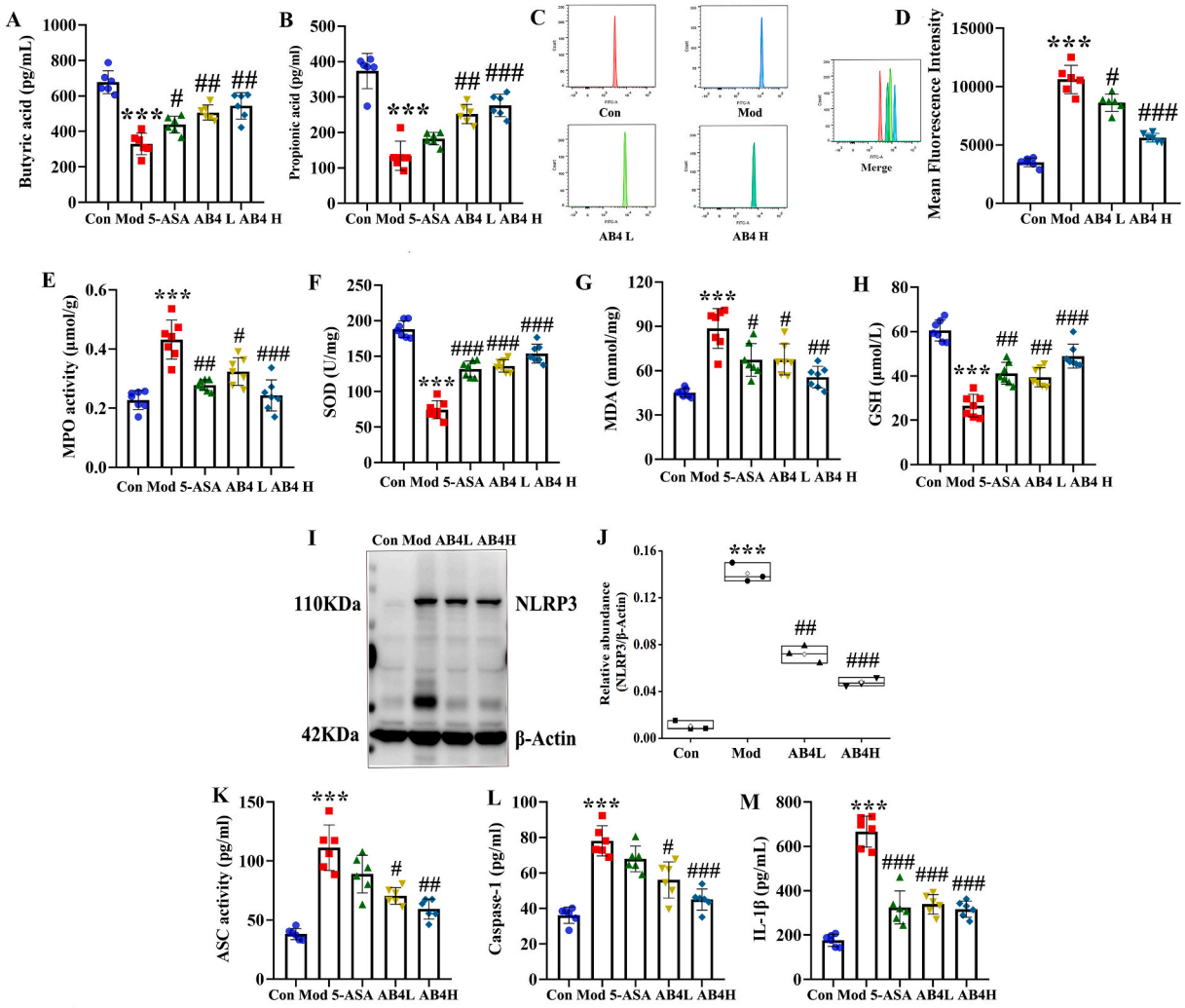

Fig. 7. AB4 inhibits oxidative stress and inflammation in UC mice. (A) The expression of butyric acid. (B) The expression of propionic acid. (C) Detection of ROS expression levels in the colon tissue by flow cytometry. (D) The mean fluorescence intensity of the colon tissue in each group. (E–H) The content of MPO, SOD, MDA and GSH in the colon tissue. (I) Western blot analysis for NLRP3 proteins in colonic tissues of colitis mice. (J) Box plot showing the densitometry analysis of NLRP3 normalized by β-Actin. (K–M) The expression level of ASC, Caspase-1 and IL-1β in colon tissue. Data are expressed as mean ± SEM for 6 mice in each group. $^{***}P < 0.001$ versus Con group, $^{\#}P < 0.05$, $^{\#\#}P < 0.01$ and $^{\#\#\#}P < 0.001$ versus Mod group.

edema, protect the morphology of intestinal mucosa, and decrease the histopathological score (Fig. 9 A). Meanwhile, AB4 obacterium fecal transplantation significantly increased the expression of ZO-1, Occludin, and Muc-2 proteins. This suggests that AB4 acts through the metabolites of the gut microbiota to alleviate intestinal inflammation and protect the intestinal barrier (Fig. 9 B). The expression of short-chain fatty acid metabolites was detected. It was found that the expression levels of intestinal propionic acid and butyric acid in mice in the FT-AB4 group were significantly higher than those in the FT-Mod group after cecal transplantation, suggesting that colony transplantation after AB4 treatment can up-regulate the expression levels of short-chain fatty acid metabolites in UC mice, which is closely related to the role of the FT-AB4 group as a treatment for UC (Fig. 9 CD).

To clarify the effect of redox reactions in treating UC with AB4 after fecal microbiota transplantation, the expression levels of redox-related indicators in the colonic tissues of mice in each group were examined. The results showed that the production of ROS in the colonic tissues of the FT-Mod group was significantly higher compared with that of the FT-Con group ($P < 0.001$). In contrast, the mice that received fecal transplantation of AB4 significantly suppressed the production of ROS ($P < 0.01$), suggesting that AB4 can inhibit ROS production through the gut microbiota short-chain fatty acids (Fig. 9 EF). The contents of MPO, SOD, MDA, and GSH were detected. The results in this part suggest that AB4 can inhibit DSS-induced intestinal oxidative stress by regulating gut microbiota short-chain fatty acid metabolites (Fig. 9G–J).

Moreover, we found that AHR is activated after FMT, which may be closely related to the antioxidant and anti-inflammatory effects of AB4 through intestinal microbial metabolites (Fig. 9 K). The expression levels of NLRP3, ASC, Caspase-1, and IL-1β were detected in the colonic tissues of mice in each group. It was found that the expression levels of NLRP3 in mice in the FT-AB4 group were substantially lower than those in the FT-Mod group ($P < 0.001$). And the mice that received fecal microbiota transplantation of AB4 significantly inhibited the expression levels of ASC, Caspase-1, and IL-1β ($P < 0.001$ or $P < 0.01$) (Fig. 9L–P). This suggests that fecal microbiota transplantation of AB4 treatment can effectively inhibit the activation of NLRP3 inflammasome and exert anti-inflammatory effects by regulating gut microbiota short-chain fatty acid metabolites.

3.8. *The gut microbiota SCFAs metabolites of AB4 improved UC mice by activating AHR*

To verify whether AB4 reduces intestinal oxidative stress and inflammation via microbial metabolites, propionic acid and butyric acid

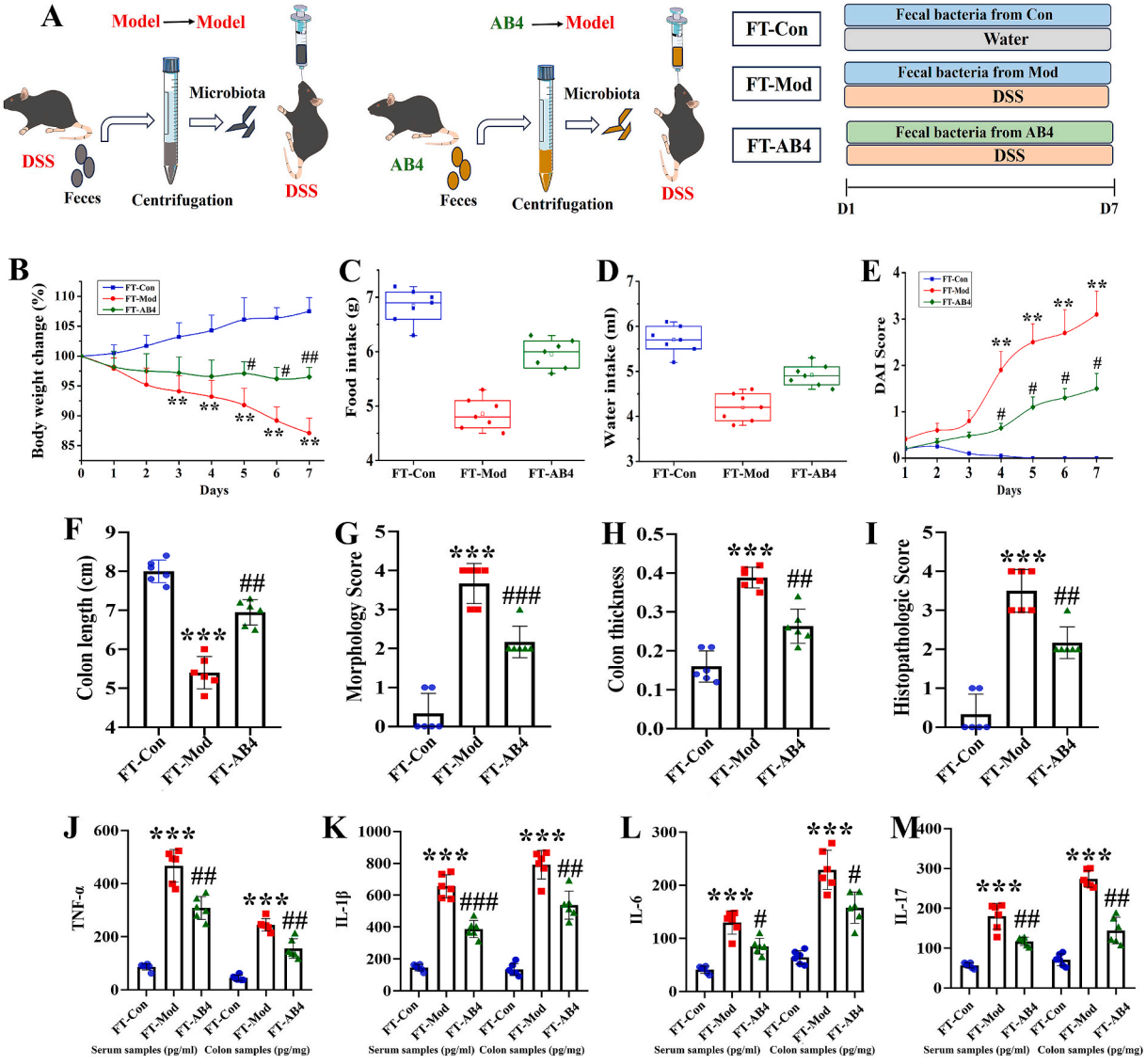

Fig. 8. Effect of AB4 on DSS-induced UC mice after fecal microbiota transplantation. (A) The flowchart of the part in vivo experiments. (B) The body weight of mice in each group. (C) The food intake. (D) The water intake. (E) DAI score. (F) Colon length. (G) Morphology score. (H) Colon thickness. (I) Histopathological score. (J–M) Inflammatory cytokines (TNF-α, IL-1β, IL-6, and IL-17) levels in colonic tissues. $^{*}P < 0.05$, $^{**}P < 0.01$ and $^{***}P < 0.001$ versus Con group, $^{\#}P < 0.05$, $^{\#\#}P < 0.01$ and $^{\#\#\#}P < 0.001$ versus Mod group.

(sodium propionate 150 mM, sodium butyrate 150 mM, administered daily via oral gavage) were used to validate the effects of two metabolites on DSS-induced UC (Fig. 10 A).

The results showed that the administration of sodium propionate and sodium butyrate, had a significant effect on dss induced UC mice, respectively. Specifically, propionate and butyrate treatment significantly increased body weight, decreased DAI scores, restored colon morphology and scores, and reduced colonic pathological damage in UC mice (Fig. 10B–G).

The contents of MPO, SOD, MDA, and GSH in the intestinal tissues of mice in each group were detected, and compared with the Con group, the contents of MPO and MDA in the Mod group were significantly higher ($P < 0.001$), and the contents of SOD and GSH were significantly lower ($P < 0.001$). Compared with the Mod group, the expression levels of MPO and MDA in the intestinal tissues of the PA and BA groups were significantly lower ($P < 0.05$ or $P < 0.01$ or $P < 0.001$), and the contents of SOD and GSH were significantly higher ($P < 0.05$ or $P < 0.01$ or $P < 0.001$). This part of the results suggested that propionic acid and butyric acid could effectively inhibit DSS-induced triggered intestinal oxidative stress (Fig. 10I–L).

Further intestinal H&E staining was performed on each group of mice, and relevant intestinal barrier indexes were observed by immunofluorescence. The results showed that propionic acid and butyric acid can reduce the infiltration of inflammation into colonic tissue, alleviate edema and mucosal epithelial damage, restore crypt structure, and have a protective effect on pathological intestinal injury. Meanwhile, it has decreased general morphological scores and histopathological scores. (Fig. 10H). Meanwhile, the protein expression of ZO-1, Occludin, and Muc-2 was analyzed by immunofluorescence, and it was found that propionic acid and butyric acid significantly increased the protein expression of ZO-1, Occludin, and Muc-2, and protected the intestinal barrier integrity. Thus, propionic acid and butyric acid replicated the ameliorative effects of AB4 on DSS-induced oxidative stress and inflammation in the intestinal tract of UC mice and exerted intestinal protection (Fig. 10 M).

The related cytokines in the colonic tissues of mice in each group were examined, and the results showed that propionic acid and butyric acid significantly inhibited the expression levels of TNF-α, IL-6, IL-17, and IL-1β after treatment (Fig. 10N–Q). Importantly, AhR levels, which were significantly reduced in the DSS group compared to the Con group,

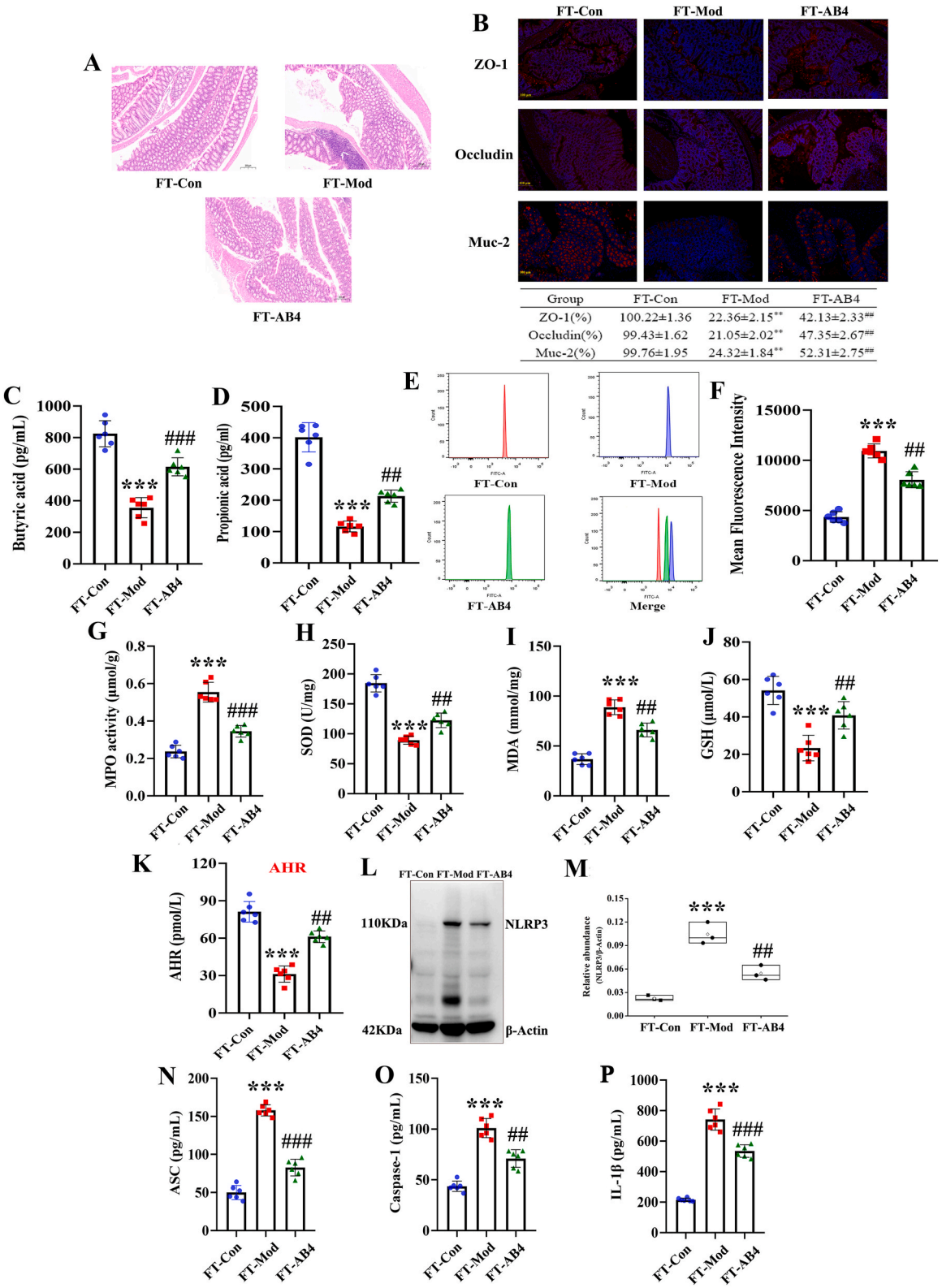

Group	FT-Con	FT-Mod	FT-AB4
ZO-1(%)	100.22±1.36	22.36±2.15**	42.13±2.33##
Occludin(%)	99.43±1.62	21.05±2.02**	47.35±2.67##
Muc-2(%)	99.76±1.95	24.32±1.84**	52.31±2.75##

Fig. 9. AB4 attenuates UC in a gut microbiota short-chain fatty acid metabolites-dependent manner and activating AHR. (A) Representative H&E images for colonic tissues. (B) Representative immunofluorescence images of ZO-1, Occludin, and Muc-2 in colonic tissues (n = 3). (C) The expression of butyric acid. (D) The expression of propionic acid. (E) Detection of ROS expression levels in the colonic tissue by flow cytometry. (F) The mean fluorescence intensity of the colonic tissue in each group. (G–J) The content of MPO, SOD, MDA and GSH in the colonic tissue. (K) The expression of AHR in the colonic tissue. (L) Western blot analysis for NLRP3 proteins in colonic tissues of colitis mice. (M) Box plot showing the densitometry analysis of NLRP3 normalized by β-Actin. (N–P) The expression level of ASC, Caspase-1 and IL-1β in colon tissue. Data are expressed as mean ± SEM for 6 mice in each group. ***$P < 0.001$ versus Con group, $^{\#\#}P < 0.01$ and $^{\#\#\#}P < 0.001$ versus Mod group.

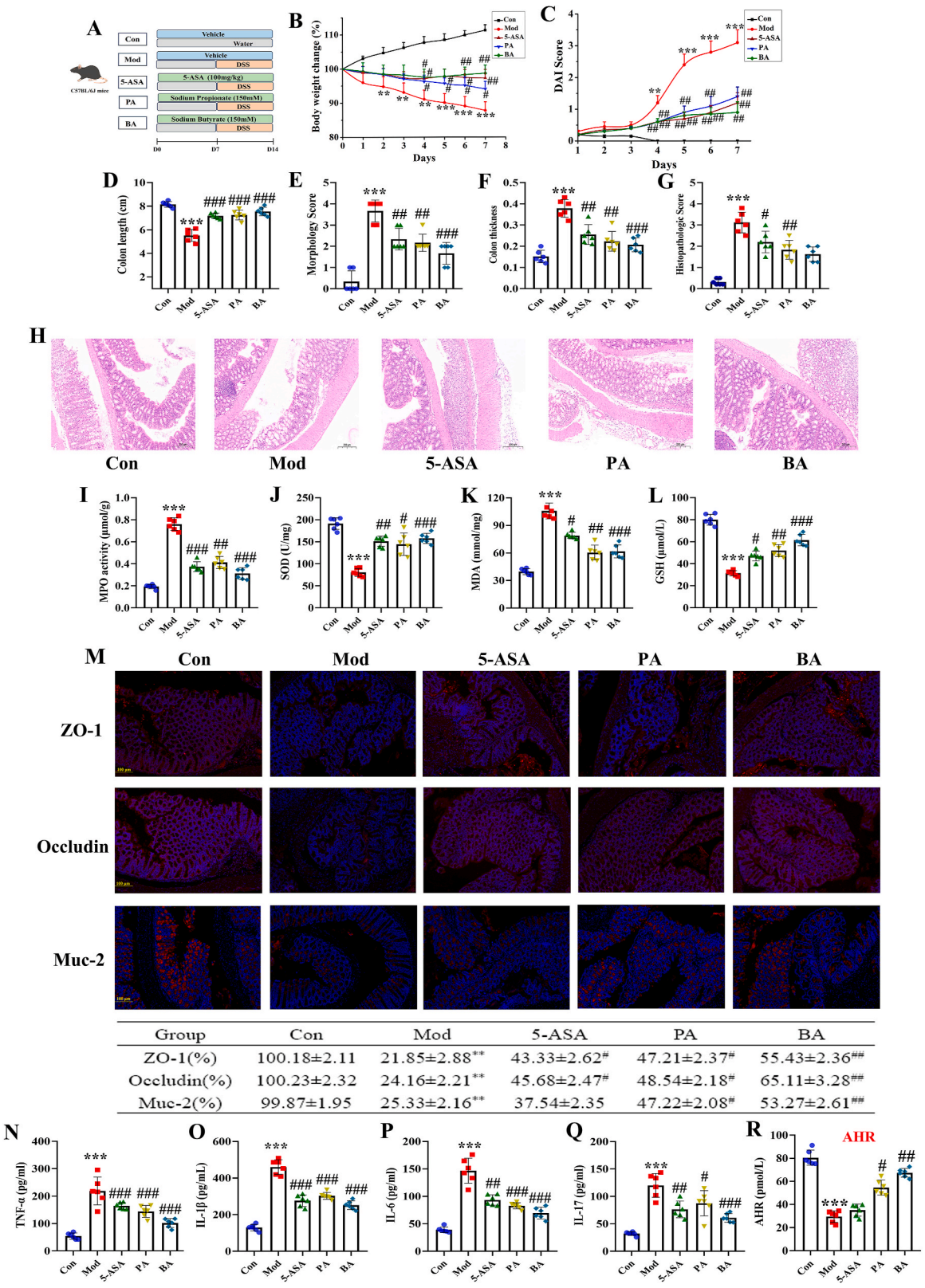

Group	Con	Mod	5-ASA	PA	BA
ZO-1(%)	100.18±2.11	21.85±2.88**	43.33±2.62#	47.21±2.37#	55.43±2.36##
Occludin(%)	100.23±2.32	24.16±2.21**	45.68±2.47#	48.54±2.18#	65.11±3.28##
Muc-2(%)	99.87±1.95	25.33±2.16**	37.54±2.35	47.22±2.08#	53.27±2.61##

Fig. 10. The gut microbiota SCFAs metabolites of AB4 improved UC mice by activating AHR. (A) The flowchart of the part in vivo experiments. (B) The body weight of mice in each group. (C) DAI score. (D) Colon length. (E) Morphology score. (F) Colon thickness. (G) Histopathological score. (H) Representative H&E images for colonic tissues. (I–L) The content of MPO, SOD, MDA and GSH in the colon tissue. (M) Representative immunofluorescence images of ZO-1, Occludin, and Muc-2 in colonic tissues (n = 3). (N–Q) Inflammatory cytokines (TNF-α, IL-1β, IL-6, and IL-17) levels in colonic tissues. (R) The expression of AHR in the colonic tissue. Data are expressed as mean ± SEM for 6 mice in each group. $^{*}P < 0.05$, $^{**}P < 0.01$ and $^{***}P < 0.001$ versus Con group, $^{\#}P < 0.05$, $^{\#\#}P < 0.01$ and $^{\#\#\#}P < 0.001$ versus Mod group.

were notably restored following PA and BA treatment (Fig. 10 R).

3.9. Butyric acid protects intestinal organoids damaged by DSS on activating AHR

A DSS-induced intestinal organoids damage model was used to confirm further the effect of BA in inhibiting oxidative stress and alleviating intestinal inflammation. We observed a dose-dependent increase in intestinal organoid viability after 10 h of co-incubation with 2–8 μM BA. However, when the concentration of BA was more significant than 8 μM, BA significantly inhibited the viability of intestinal organoids compared. After that, the intestinal organoids were incubated with DSS (0.1 %) and BA (1–32 μM) for 10 h. We found that BA dose-dependently inhibited DSS-induced damage to intestinal organoids in the dose range of 2–8 μM (Fig. S1). Therefore, we chose BA concentrations of 2, 4, and 8 μm as the experimental doses to explore the effects of BA on the regulation of oxidative stress and inflammation in the DSS-induced intestinal organoid model.

Exposure of organoids to DSS resulted in 3D culture organoid disintegration and enterocyte apoptosis. Importantly, BA significantly inhibited organoid disintegration and reduced apoptosis, suggesting that BA prevents DSS-induced organoid damage (Fig. 11 A). Similar results for the anti-inflammatory effects of BA were observed in the DSS-induced organoid model, where DSS intervention in organoids significantly increased the secretion of IL-6, IL-1β, IL-17, and TNF-α cytokines, which were dose-dependently inhibited by treatment with BA (Fig. 11B–E).

At the same time, we found that DSS inhibited the expression of AHR in intestinal organoids, and BA protected the intestine by activating AHR (Fig. 11 F). The high-dose group of BA was further selected for ROS production detection, and the ROS production in each group's supernatant was detected by flow cytometry 24 h after the intervention. The results suggested that DSS stimulation of the intestinal organoid model could significantly increase ROS production. At the same time, BA treatment could effectively inhibit ROS production (Fig. 11 GH). The expressions of NLRP3, ASC, Caspase-1, and IL-1β were detected in the lysates of organoid in each group. The results showed that treatment with BA significantly inhibited the activation of NLRP3 inflammasome in intestinal organoid lysates exposed to DSS, suggesting a better anti-inflammatory effect for treating UC (Fig. 11I–M).

3.10. AhR is a key target that mediates the Anti-UC effect of AB4

Previous studies have shown that SCFAs and its derivatives, which are produced through microbial regulation of SCFAs metabolism, can prevent colitis by binding to and activating AhR as ligands, suggesting that AB4 may alleviate colitis by enriching the gut microbiota, thereby triggering AhR activation from the metabolite BA. To confirm this hypothesis, we exposed DSS treated mice to AhR inhibitors to verify the contribution of AhR to the anti-UC efficacy of AB4. Specifically, AB4 treatment increased body weight considerably, decreased DAI scores, restored colon morphology and decreased general morphological scores and histopathological scores, and reduced colonic pathological damage in UC mice. Still, the expression had no therapeutic effect on UC mice after combined AhR antagonist (Fig. 12A–G). AhR antagonist completely abolished the ameliorating effects of AB4 and BA on colitis, including MPO, SOD, MDA, GSH, TNF-α, IL-1β, IL-6, and IL-17 (Fig. 12H–P). Interestingly, we found that the protective effect of AB4 on the intestinal barrier disappeared after the addition of AHR inhibitors (Fig. 12 Q). It is suggested that the role of AB4 in protecting the intestinal barrier function is mainly mediated by activating AHR.

4. Discussion

Ulcerative colitis (UC) is a non-specific inflammatory disease of uncertain etiology with a prolonged and recurrent course. The incidence of UC is rising with increasing social and economic development [3,4,6]. Since oxidative stress and inflammation are significant factors in UC, the potential of natural products in IBD therapy is gaining attention [42]. AB4 significantly reduced symptoms in UC mouse models, as demonstrated by inhibiting intestinal oxidative stress and inflammation and improving intestinal barrier integrity. Besides, We found that the high-dose AB4 group (AB4 H) exhibited better anti-inflammatory activity than 5-ASA (TNF-α, IL-6 and IL-17), it might suggest that AB4 has a superior anti-inflammatory effect. In addition, AB4 modified the gut microbiota in UC mice (increasing *Lactobacillus*), thereby promoting the production of the short-chain fatty acid metabolite BA. Subsequent experiments showed that BA effectively restored tight junction protein levels in UC mice and reduced intestinal oxidative stress and inflammation. Tight junction proteins are composed of multi-protein complexes, including cytoplasmic proteins, ZO-1 and occludin. ZO proteins and occludin play an important role in the permeability and adhesion of epithelial cells and signal transduction. The down-regulation of its expression or the decrease of its activity will affect the formation of tight junctions [55,56]. In this study, it was found through immunofluorescence that both AB4 and BA could restore the decreased expression of ZO-1 and occludin after DSS induction, and the protein expression levels could still be further verified by Western blot.

This anti-inflammatory effect is mediated by the activation of the AHR pathway by AB4 and BA. AB4 regulates the gut microbiome to enhance BA production, thereby activating AHR, inhibiting oxidative stress and inflammation, improving gut barrier integrity, and ultimately reducing UC symptoms. At the same time, liver and kidney function indices were also tested on the 14th day after rectal administration, and histopathological changes in the liver and kidney were observed. The results showed that AB4 had no significant effect on liver and kidney functions compared to the control group. Histopathological results showed that after rectal administration of 100 mg/kg AB4, the liver and kidney tissues of mice were structurally normal, the epithelial cells were neatly arranged, and no inflammatory infiltration or pathological changes were observed (Fig. S2).

In recent years, the close relationship between gut microbial dysbiosis and the pathogenesis of UC has become one of the hotspots of medical research [13,15]. An imbalance in the composition of gut microorganisms can either directly cause UC or modulate the pathogenesis of UC through the metabolites of gut microbes [16,18]. In this study, from the results of 16S rRNA sequencing, we found that AB4 effectively improved the α and β diversity of the gut microbial in UC mice. The species composition was more similar to that of normal mice after AB4 treatment. The MDI index also showed that AB4 treatment significantly adjusted the gut microbial disorder caused by DSS. At the phylum level, AB4 improved the abundance of *Bacteroidota* and *Firmicutes*, the key dominant species of the gut microbial. Further examination of the relative abundance of microorganisms at the genus level revealed that AB4 significantly increased the abundance of *Lactobacillus* and decreased the abundance of *Muribaculaceae*. As a probiotic, *Lactobacillus* can alleviate many diseases, reduce intestinal inflammation, and maintain a healthy intestinal barrier. Finally, after AB4 treatment, the Lefse multilevel species difference discriminant analysis and PICRUSt2 functional prediction analyzed microbial taxa and functional information, suggesting that the flora alterations are closely related to redox-related pathways. This part of the results indicates that gut microbes may be essential in inhibiting UC inflammation by AB4.

In this study, we analyzed the gut metabolites of AB4-treated UC by non-target metabolomics, and the results showed that the primary metabolic pathway involved was short-chain fatty acid metabolism. The gut microbial is the largest intestinal micro-ecosystem in the human body. SCFAs are metabolites produced by the gut microbial involved in the fermentation of proteins and carbohydrates in the intestinal tract, inhibiting intestinal inflammatory responses. Whereas SCFAs have become a promising strategy for treating UC, it has been shown that propionate inhibited the down-regulation of tight junction proteins and

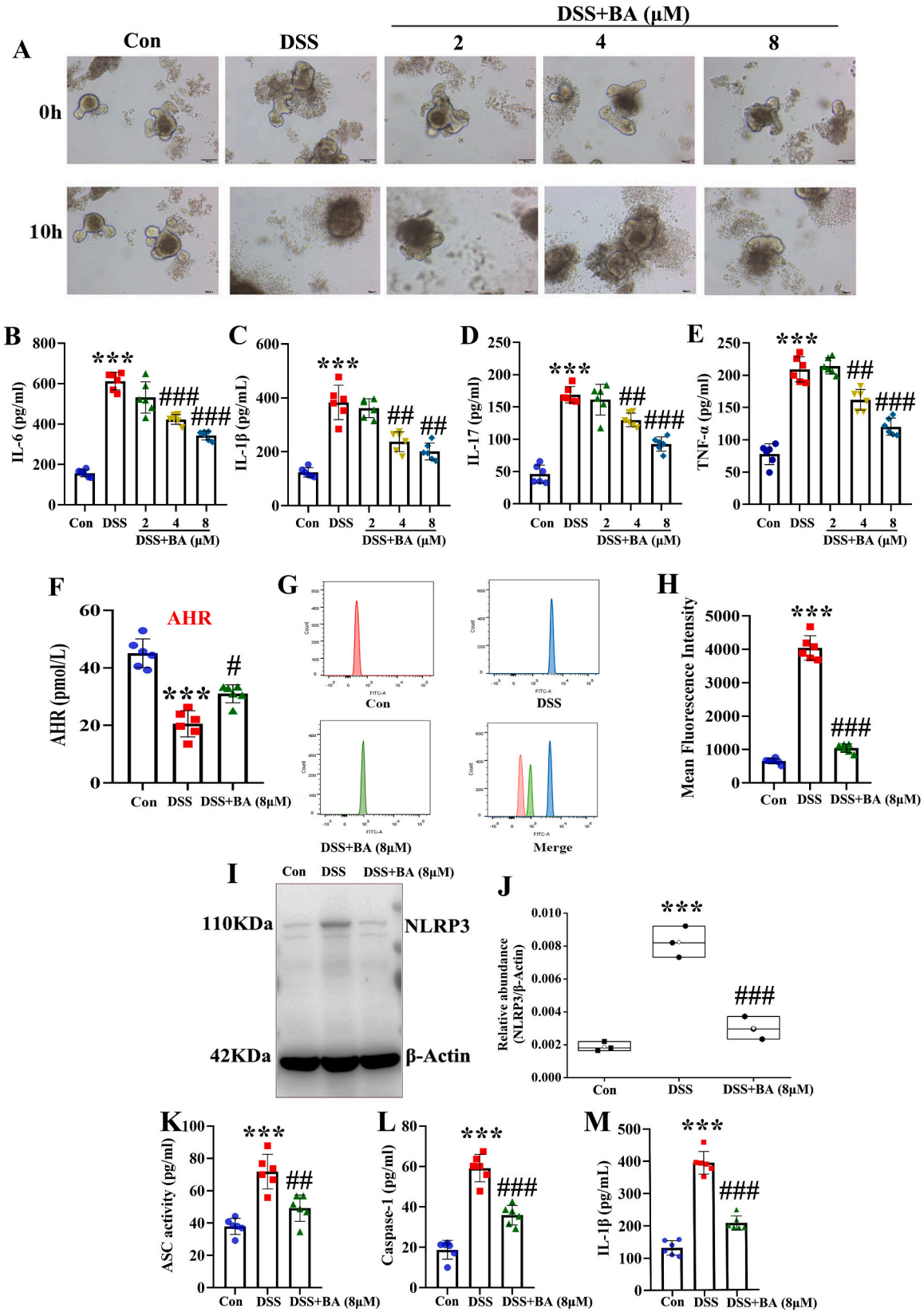

Fig. 11. Butyric acid protects intestinal organoids damaged by DSS on activating AHR. (A) The morphological change of intestinal organoids in DSS stimulation. (B–E) The levels of pro-inflammatory cytokines (IL-1β, IL-6, IL-17, and TNF-α) in the supernatant. (F) The expression of AHR. (G) Detection of ROS expression levels by flow cytometry. (H) The mean fluorescence intensity in each group. (I) Western blot analysis for NLRP3 proteins in intestinal organoids. (J) Box plot showing the densitometry analysis of NLRP3 normalized by β-Actin. (K–M) The expression level of ASC, Caspase-1 and IL-1β in intestinal organoids. $^{***}P < 0.001$ versus Con group, $^{\#\#}P < 0.01$ and $^{\#\#\#}P < 0.001$ versus Mod group.

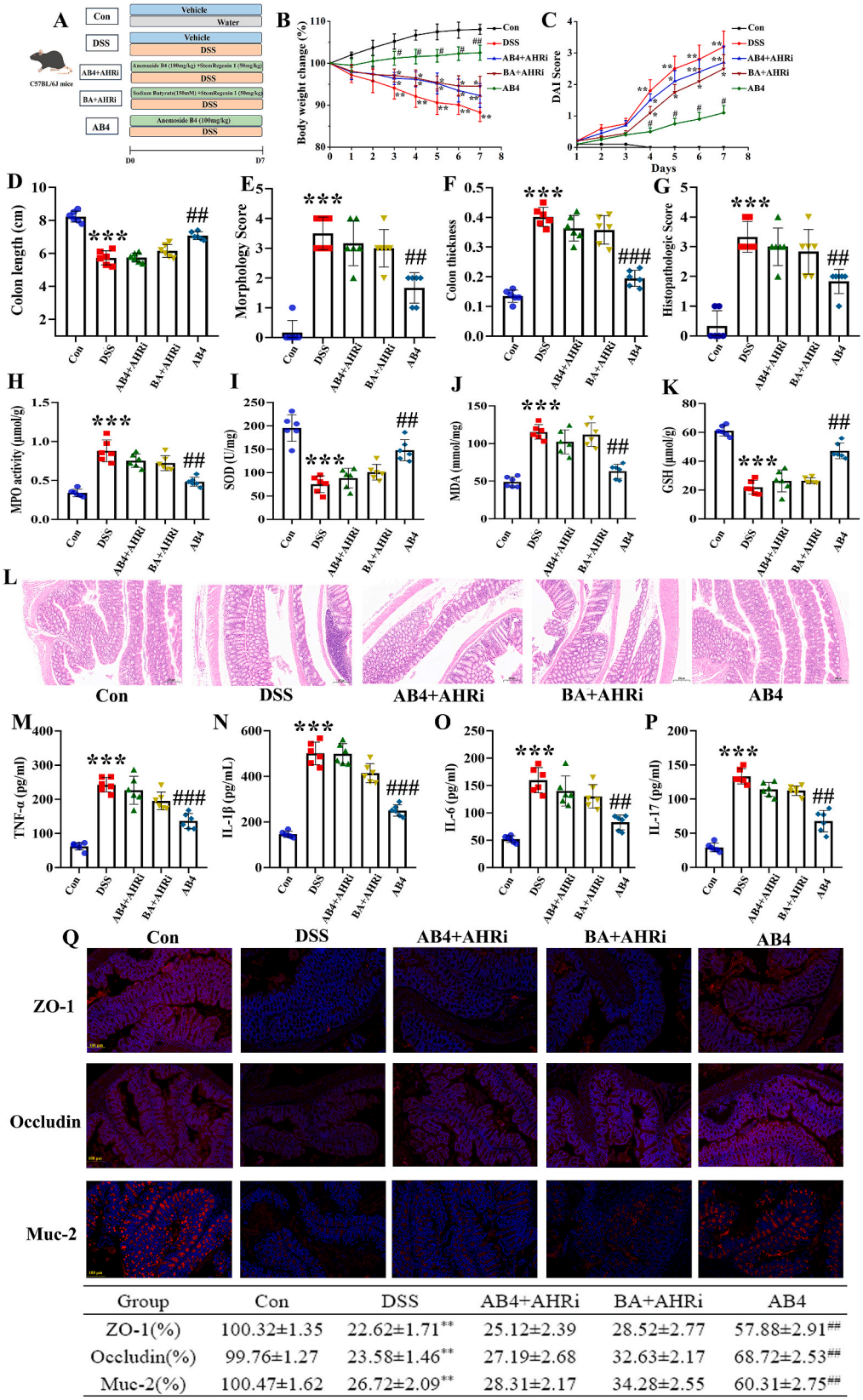

Group	Con	DSS	AB4+AHRi	BA+AHRi	AB4
ZO-1(%)	100.32±1.35	22.62±1.71**	25.12±2.39	28.52±2.77	57.88±2.91##
Occludin(%)	99.76±1.27	23.58±1.46**	27.19±2.68	32.63±2.17	68.72±2.53##
Muc-2(%)	100.47±1.62	26.72±2.09**	28.31±2.17	34.28±2.55	60.31±2.75##

Fig. 12. AhR is a key target that mediates the anti-UC effect of AB4. (A) The flowchart of the part in vivo experiments. (B) The body weight of mice in each group. (C) DAI score. (D) Colon length. (E) Morphology score. (F) Colon thickness. (G) Histopathological score. (H–K) The expression of MPO, SOD, MDA, and GSH. (L) Representative H&E images for colonic tissues. (M–P) Inflammatory cytokines (TNF-α, IL-1β, IL-6, and IL-17) levels in colonic tissues. (O) Representative immunofluorescence images of ZO-1, Occludin, and Muc-2 in colonic tissues (n = 3). Data are expressed as mean ± SEM for 6 mice in each group. $^{*}P < 0.05$, $^{**}P < 0.01$ and $^{***}P < 0.001$ versus Con group, $^{\#}P < 0.05$, $^{\#\#}P < 0.01$ and $^{\#\#\#}P < 0.001$ versus Mod group.

ameliorated DSS-induced intestinal barrier dysfunction. And propionate inhibited the oxidative stress in the colon by decreasing the activity of MPO and augmenting the activity of SOD and CAT in the serum and colon [57]. In clinical studies, UC patients have been found to have a reduced abundance of beneficial bacteria in the gut microbial, mainly *Faecalibacterium* and genera associated with butyrate acid production [58]. Whereas SCFA metabolism was the most enriched pathway in this study, we focused on SCFA metabolites to investigate the possible mechanisms further.

As an essential metabolite that can reflect the microbiological function of gut microbes, SCFA can provide energy for intestinal epithelial cells and play a crucial role in maintaining the normal morphology and structure of intestinal epithelial cells and regulating the homeostasis of the intestinal microenvironment [24–26]. Our metabolomics analysis confirmed a significant increase in BA levels after AB4 treatment. SCFAs, including BA, are considered ligands of AHR, key regulators of intestinal immunity, and key players in initiating downstream signaling pathways [28–30]. In addition, our study showed that after significant activation of AHR, ROS production could be effectively regulated, and the expression levels of MPO, SOD, MDA and GSH could be affected, thus inhibiting oxidative stress. At the same time, AHR activation effectively reduced the activation of the NLRP3 inflammasome in the intestinal tissue of UC mice, inhibited the related inflammatory response, and protected the intestinal barrier. Meanwhile,We used immunohistochemistry to assess the positive expression of Caspase-1 and GSDMD in colon tissue from UC mice after AB4 treatment. The results showed that Caspase-1 and GSDMD expressions were significantly upregulated in the colon tissue of UC group mice ($P < 0.05$), while AB4 significantly inhibited Caspase-1 and GSDMD expressions ($P < 0.05$), suggesting that AB4 may exert its therapeutic effect by inhibiting activated Caspase-1, thereby regulating GSDMD and inflammatory factor expression levels, and suppressing intestinal epithelial cell pyroptosis to improve intestinal inflammation (Fig. S3).

In this study, it was found that the gut microbiota and its metabolites BA are central to the anti-UC effects of AB4. BAs can influence intestinal barrier function by regulating immune responses, which may indirectly modify the composition of the intestinal bacterial community. Research has shown that supplementing with BAs can significantly upregulate the expression of tight junction proteins in the gut, enhance the barrier function of the intestinal mucosa, and help maintain its integrity. This supplementation might also influence the gut microbiota [59,60]. On one hand, the structure of the gut microbiota determines BA production. The concentrations of BAs in the gut are affected by the composition and proportions of gut commensal bacteria. Dysbiosis can lead to changes in butyrate levels [61]. On the other hand, the concentration of butyrate can inversely regulate the structure of the microbiota. Oral administration of BAs has been shown to reduce the abundance of butyrate-producing bacteria such as *Lachnospiraceae blautia*, *Lachnospiraceae marvinbryantia*, and *Faecalibacterium prausnitzii* [62]. Meanwhile, BA treatment increases the abundance of certain microorganisms, including *Acinetobacter*, *Facklamia*, *Kocuria*, and *Rothia* [63]. This suggests that BA supplementation may regulate the composition and activity of gut microbiota through feedback mechanisms or by modulating the gene expression of microorganisms involved in BA production.

Furthermore, FMT confirmed that AB4's protective effect on UC mice is mediated by SCFAs derived from intestinal microbiota, which activate the AHR. When the intestinal flora from DSS-treated mice that had been given AB4 was transplanted into recipient Mod mice, there was a significant increase in BA levels, and AHR was activated. This activation effectively alleviated UC-related symptoms, reduced the pathological damage caused by DSS to the colon of the mice, and protected the intestinal barrier function. These findings suggest that AB4's activation of AHR not only inhibits intestinal inflammation but also influences intestinal homeostasis and the composition of the intestinal bacterial community. By regulating the intestinal microbiota and its metabolic products, AB4-mediated AHR activation further enhances AHR expression and maintains the integrity of the intestinal barrier. Additionally, the introduction of an AHR inhibitor weakened the therapeutic effect of AB4 on UC, which may be closely related to changes in the composition of the microbiota.

Both AB4 and BA treatments significantly increased the expression levels of AHR in the colon, inhibited pro-inflammatory cytokines, and repaired intestinal barrier function. Activation of AHR by AB4 was found to suppress intestinal inflammation and promote intestinal homeostasis, as well as remodeling of the intestinal bacterial community. Notably, the use of AHR antagonists eliminated the beneficial effects of BA on colitis and also diminished the effects of AB4. Given this discrepancy, we hypothesize that AB4's ability to alleviate colitis may stem from multiple mechanisms. For instance, our metabolomics findings suggest that AB4 also modulates arginine signaling, which may play a role in its anti-inflammatory effects in ulcerative colitis. While BA is one of the key metabolites produced by AB4, and its efficacy has been demonstrated in the treatment of UC, the functions of other metabolites regulated by AB4 remain unclear. Although our study showed that AB4 modulates the microbiota, further research is necessary to identify additional bacterial species capable of producing short-chain fatty acids, such as BA. This understanding is crucial for comprehensively delineating the anti-UC mechanisms of AB4 and advancing its development as a therapeutic agent.

In conclusion, our findings indicate that AB4 regulates the gut microbiome to increase BA production, which in turn activates the AHR. This process helps to reduce intestinal oxidative stress and inflammation, enhance gut barrier integrity, and ultimately alleviate symptoms of UC. Our study presents a novel mechanism by which AB4 offers protective effects against UC. The data we have collected may contribute to the development of promising treatments for UC by targeting specific metabolites or bacteria to improve the condition.

CRediT authorship contribution statement

Hao Wu: Writing – original draft, Supervision, Software, Formal analysis, Data curation, Conceptualization. **Yao-lei Li:** Software, Resources, Methodology, Investigation. **Yu Wang:** Validation, Software, Methodology, Formal analysis. **Yu-ge Wang:** Resources, Methodology, Formal analysis, Data curation. **Jia-hui Hong:** Software, Resources, Formal analysis. **Mi-mi Pang:** Writing – review & editing, Resources, Project administration, Methodology, Data curation. **Pan-miao Liu:** Writing – review & editing, Validation, Investigation, Formal analysis, Data curation. **Jian-jun Yang:** Writing – review & editing, Funding acquisition, Formal analysis, Data curation, Conceptualization.

Data availability

The data that support the findings of this study are available from the corresponding author upon reasonable request.

Declaration of competing interest

The authors declare that they have no known competing financial interests or personal relationships that could have appeared to influence the work reported in this paper.

Acknowledgments

This work was supported by the State-sponsored Postdoctoral Researcher Program of China (GZC20232422), the Joint Construction Project of Henan Province Medical Science and Technology Research Program (LHGJ20240249), the National Natural Science Foundation of China (No. U23A20421) and the Natural Science Foundation of Henan Province (No. 252300420544).

Appendix A. Supplementary data

Supplementary data to this article can be found online at https://doi.org/10.1016/j.redox.2025.103746.

Data availability

Data will be made available on request.

References

[1] I. Ordás, L. Eckmann, M. Talamini, D.C. Baumgart, W.J. Sandborn, Ulcerative colitis, Lancet 380 (9853) (2012 Nov 3) 1606–1619.
[2] J.P. Segal, J.F. LeBlanc, A.L. Hart, Ulcerative colitis: an update, Clin. Med. 21 (2) (2021 Mar) 135–139.
[3] R. Voelker, What is ulcerative colitis? JAMA 331 (8) (2024 Feb 27) 716.
[4] M. Eisenstein, Ulcerative colitis: towards remission, Nature 563 (7730) (2018 Nov) S33.
[5] P. Wangchuk, K. Yeshi, A. Loukas, Ulcerative colitis: clinical biomarkers, therapeutic targets, and emerging treatments, Trends Pharmacol. Sci. 45 (10) (2024 Oct) 892–903.
[6] Y. Sun, Z. Zhang, C.Q. Zheng, L.X. Sang, Mucosal lesions of the upper gastrointestinal tract in patients with ulcerative colitis: a review, World J. Gastroenterol. 27 (22) (2021 Jun 14) 2963–2978.
[7] K.K. Cho, Y. Ko, K. Nilsen, C. Verdon, G. Femia, Ulcerative colitis and acute perimyocarditis, Med. J. Aust. 216 (11) (2022 Jun 20) 559–561.
[8] F. D'Amico, L. Peyrin-Biroulet, S. Danese, Disease clearance in ulcerative colitis: is the ultimate therapeutic target? United European Gastroenterol J 11 (8) (2023 Oct) 717–719.
[9] J. Torres, V. Billioud, D.B. Sachar, L. Peyrin-Biroulet, J.F. Colombel, Ulcerative colitis as a progressive disease: the forgotten evidence, Inflamm. Bowel Dis. 18 (7) (2012 Jul) 1356–1363.
[10] I. Marafini, J. Roseira, M. Duijvestein, Treatment options for refractory ulcerative colitis: small molecules, big effects, United European Gastroenterol J 12 (5) (2024 Jun) 539–540.
[11] C. Klotz, M. Barret, M. Dhooge, A. Oudjit, S. Chaussade, R. Coriat, V. Abitbol, Rectocolite hémorragique : conduite diagnostique et prise en charge thérapeutique Management of diagnosis and treatment in ulcerative colitis, Presse Med. 44 (2) (2015 Feb) 144–149.
[12] D. Con, A. Vasudevan, D.R. van Langenberg, Predictive scores in acute severe ulcerative colitis: which, what, and when are the decision points we should target? Clin. Gastroenterol. Hepatol. 20 (2) (2022 Feb) e344–e345.
[13] M.X. Li, M.Y. Li, J.X. Lei, Y.Z. Wu, Z.H. Li, L.M. Chen, C.L. Zhou, J.Y. Su, G. X. Huang, X.Q. Huang, X.B. Zheng, Huangqin decoction ameliorates DSS-Induced ulcerative colitis: role of gut microbiota and amino acid metabolism, mTOR pathway and intestinal epithelial barrier, Phytomedicine 100 (2022 Jun) 154052.
[14] B. Li, P. Du, Y. Du, D. Zhao, Y. Cai, Q. Yang, Z. Guo, Luteolin alleviates inflammation and modulates gut microbiota in ulcerative colitis rats, Life Sci. 269 (2021 Mar 15) 119008.
[15] H. Cheng, J. Liu, D. Zhang, J. Wang, Y. Tan, W. Feng, C. Peng, Ginsenoside Rg1 alleviates acute ulcerative colitis by modulating gut microbiota and microbial tryptophan metabolism, Front. Immunol. 13 (2022 May 17) 817600.
[16] L. Tong, H. Hao, Z. Zhang, Y. Lv, X. Liang, Q. Liu, T. Liu, P. Gong, L. Zhang, F. Cao, G. Pastorin, C.N. Lee, X. Chen, J.W. Wang, H. Yi, Milk-derived extracellular vesicles alleviate ulcerative colitis by regulating the gut immunity and reshaping the gut microbiota, Theranostics 11 (17) (2021 Jul 25) 8570–8586.
[17] Rhein modulates host purine metabolism in intestine through gut microbiota and ameliorates experimental colitis, Theranostics 10 (23) (2020 Aug 29) 10665–10679.
[18] J. Zhang, F. Gao, Anti-inflammatory effect of rhein on ulcerative colitis via inhibiting PI3K/Akt/mTOR signaling pathway and regulating gut microbiota, Phytother Res. 36 (5) (2022 May) 2081–2094.
[19] X. Wang, S. Huang, M. Zhang, Y. Su, Z. Pan, J. Liang, X. Xie, Q. Wang, J. Chen, L. Zhou, X. Luo, Gegen Qinlian decoction activates AhR/IL-22 to repair intestinal barrier by modulating gut microbiota-related tryptophan metabolism in ulcerative colitis mice, J. Ethnopharmacol. 302 (Pt B) (2023 Feb 10) 115919.
[20] P. Guo, W. Wang, Q. Xiang, C. Pan, Y. Qiu, T. Li, D. Wang, J. Ouyang, R. Jia, M. Shi, Y. Wang, J. Li, J. Zou, Y. Zhong, J. Zhao, D. Zheng, Y. Cui, G. Ma, W. Wei, Engineered probiotic ameliorates ulcerative colitis by restoring gut microbiota and redox homeostasis, Cell Host Microbe 32 (9) (2024 Sep 11) 1502–1518.e9.
[21] Z. Yu, D. Li, H. Sun, Herba origani alleviated DSS-Induced ulcerative colitis in mice through remolding gut microbiota to regulate bile acid and short-chain fatty acid metabolisms, Biomed. Pharmacother. 161 (2023 May) 114409.
[22] C. Lou, X. Cao, X. Chen, B. Li, B. Wang, J. Zhao, Lactic acid-producing probiotic Saccharomyces cerevisiae attenuates ulcerative colitis via suppressing macrophage pyroptosis and modulating gut microbiota, Front. Immunol. 12 (2021 Nov 24) 777665.
[23] C. Niu, X.L. Hu, Z.W. Yuan, Y. Xiao, P. Ji, Y.M. Wei, Y.L. Hua, Pulsatilla decoction improves DSS-Induced colitis via modulation of fecal-bacteria-related short-chain fatty acids and intestinal barrier integrity, J. Ethnopharmacol. 300 (2023 Jan 10) 115741.
[24] Vila A. Vich, S. Hu, S. Andreu-Sánchez, V. Collij, B.H. Jansen, H.E. Augustijn, L. A. Bolte, R.A.A.A. Ruigrok, G. Abu-Ali, C. Giallourakis, J. Schneider, J. Parkinson, A. Al-Garawi, A. Zhernakova, R. Gacesa, J. Fu, R.K. Weersma, Faecal metabolome and its determinants in inflammatory bowel disease, Gut 72 (8) (2023 Aug) 1472–1485.
[25] Y. Hu, Z. Chen, C. Xu, S. Kan, D. Chen, Disturbances of the gut microbiota and microbiota-derived metabolites in inflammatory bowel disease, Nutrients 14 (23) (2022 Dec 2) 5140.
[26] L. Liang, L. Liu, W. Zhou, C. Yang, G. Mai, H. Li, Y. Chen, Gut microbiota-derived butyrate regulates gut mucus barrier repair by activating the macrophage/WNT/ERK signaling pathway, Clin Sci (Lond). 136 (4) (2022 Feb 25) 291–307.
[27] M. Zhao, X. Xie, B. Xu, Y. Chen, Y. Cai, K. Chen, X. Guan, C. Ni, X. Luo, L. Zhou, Paeonol alleviates ulcerative colitis in mice by increasing short-chain fatty acids derived from Clostridium butyricum, Phytomedicine 120 (2023 Nov) 155056.
[28] X. Han, R. Luo, S. Qi, Y. Wang, L. Dai, W. Nie, M. Lin, H. He, N. Ye, C. Fu, Y. You, S. Fu, F. Gao, "Dual sensitive supramolecular curcumin nanoparticles" in "advanced yeast particles" mediate macrophage reprogramming, ROS scavenging and inflammation resolution for ulcerative colitis treatment, J. Nanobiotechnol. 21 (1) (2023 Sep 7) 321.
[29] Y. Chen, P. Zhang, W. Chen, G. Chen, Ferroptosis mediated DSS-Induced ulcerative colitis associated with Nrf2/HO-1 signaling pathway, Immunol. Lett. 225 (2020 Sep) 9–15.
[30] Y. Wan, L. Yang, S. Jiang, D. Qian, J. Duan, Excessive apoptosis in ulcerative colitis: crosstalk between apoptosis, ROS, ER stress, and intestinal homeostasis, Inflamm. Bowel Dis. 28 (4) (2022 Mar 30) 639–648.
[31] H. Guo, H. Guo, Y. Xie, Y. Chen, C. Lu, Z. Yang, Y. Zhu, Y. Ouyang, Y. Zhang, X. Wang, Mo3Se4 nanoparticle with ROS scavenging and multi-enzyme activity for the treatment of DSS-Induced colitis in mice, Redox Biol. 56 (2022 Oct) 102441.
[32] L.C. Tong, Y. Wang, Z.B. Wang, W.Y. Liu, S. Sun, L. Li, D.F. Su, L.C. Zhang, Propionate ameliorates dextran sodium sulfate-induced colitis by improving intestinal barrier function and reducing inflammation and oxidative stress, Front. Pharmacol. 7 (2016) 253.
[33] Z. Wang, J. Liu, F. Li, S. Ma, L. Zhao, P. Ge, H. Wen, Y. Zhang, X. Liu, Y. Luo, J. Yao, G. Zhang, H. Chen, Mechanisms of qingyi decoction in severe acute pancreatitis-associated acute lung injury via gut microbiota: targeting the short-chain fatty acids-mediated AMPK/NF-κB/NLRP3 pathway, Microbiol. Spectr. 11 (4) (2023 Aug 17) e0366422.
[34] B. Guan, J. Tong, H. Hao, Z. Yang, K. Chen, H. Xu, A. Wang, Bile acid coordinates microbiota homeostasis and systemic immunometabolism in cardiometabolic diseases, Acta Pharm. Sin. B 12 (5) (2022 May) 2129–2149.
[35] K. Wu, Y. Yuan, H. Yu, X. Dai, S. Wang, Z. Sun, F. Wang, H. Fei, Q. Lin, H. Jiang, T. Chen, The gut microbial metabolite trimethylamine N-oxide aggravates GVHD by inducing M1 macrophage polarization in mice, Blood 136 (4) (2020 Jul 23) 501–515.
[36] N. Gasaly, M.A. Hermoso, M. Gotteland, Butyrate and the fine-tuning of colonic homeostasis: implication for inflammatory bowel diseases, Int. J. Mol. Sci. 22 (6) (2021 Mar 17) 3061.
[37] Y. Fu, J. Lyu, S. Wang, The role of intestinal microbes on intestinal barrier function and host immunity from a metabolite perspective, Front. Immunol. 14 (2023 Oct 9) 1277102, https://doi.org/10.3389/fimmu.2023.1277102.
[38] E.C. Rosser, C.J.M. Piper, D.E. Matei, P.A. Blair, A.F. Rendeiro, M. Orford, D. G. Alber, T. Krausgruber, D. Catalan, N. Klein, J.J. Manson, I. Drozdov, C. Bock, L. R. Wedderburn, S. Eaton, C. Mauri, Microbiota-derived metabolites suppress arthritis by amplifying aryl-hydrocarbon receptor activation in regulatory B cells, Cell Metab. 31 (4) (2020 Apr 7) 837–851.e10.
[39] C.H. Wiegman, F. Li, B. Ryffel, D. Togbe, K.F. Chung, Oxidative stress in ozone-induced chronic lung inflammation and emphysema: a facet of chronic obstructive pulmonary disease, Front. Immunol. 11 (2020 Sep 2) 1957.
[40] K. Walter Bock, Aryl hydrocarbon receptor (AHR): towards understanding intestinal microbial ligands including vitamin B12 and folic acid as natural antagonists, Biochem. Pharmacol. 214 (2023 Aug) 115658.
[41] P. Shaw, A. Chattopadhyay, Nrf2-ARE signaling in cellular protection: mechanism of action and the regulatory mechanisms, J. Cell. Physiol. 235 (4) (2020 Apr) 3119–3130.
[42] J.C. Xue, S. Yuan, H. Meng, X.T. Hou, J. Li, H.M. Zhang, L.L. Chen, C.H. Zhang, Q. G. Zhang, The role and mechanism of flavonoid herbal natural products in ulcerative colitis, Biomed. Pharmacother. 158 (2023 Feb) 114086.
[43] R.P.D. Nascimento, A.P.D.F. Machado, J. Galvez, C.B.B. Cazarin, M.R. Maróstica Junior, Ulcerative colitis: gut microbiota, immunopathogenesis and application of natural products in animal models, Life Sci. 258 (2020 Oct 1) 118129.
[44] W. Zhang, M. Zou, J. Fu, Y. Xu, Y. Zhu, Autophagy: a potential target for natural products in the treatment of ulcerative colitis, Biomed. Pharmacother. 176 (2024 Jul) 116891.
[45] Y. Ruan, X. Zhu, J. Shen, H. Chen, G. Zhou, Mechanism of nicotiflorin in san-ye-qing rhizome for anti-inflammatory effect in ulcerative colitis, Phytomedicine 129 (2024 Jul) 155564.
[46] J. Zhong, L. Tan, M. Chen, C. He, Pharmacological activities and molecular mechanisms of pulsatilla saponins, Chin. Med. 17 (1) (2022 May 23) 59.
[47] L. Lv, Q. Li, K. Wang, J. Zhao, K. Deng, R. Zhang, Z. Chen, I.A. Khan, C. Gui, S. Feng, S. Yang, Y. Liu, Q. Xu, Discovery of a new anti-inflammatory agent from anemoside B4 derivatives and its therapeutic effect on colitis by targeting pyruvate carboxylase, J. Med. Chem. 67 (9) (2024 May 9) 7385–7405.
[48] R. Yuan, J. He, L. Huang, L.J. Du, H. Gao, Q. Xu, S. Yang, Anemoside B4 protects against acute lung injury by attenuating inflammation through blocking NLRP3 inflammasome activation and TLR4 dimerization, J Immunol Res 2020 (2020 Dec 3) 7502301.

[49] S. Chu, D. Shan, L. He, S. Yang, Y. Feng, Y. Zhang, J. Yu, Anemoside B4 attenuates abdominal aortic aneurysm by limiting smooth muscle cell transdifferentiation and its mediated inflammation, Front. Immunol. 15 (2024 May 31) 1412022.
[50] L. Shen, H. Luo, L. Fan, Z. Su, S. Yu, S. Cao, X. Wu, Exploration of the immuno-adjuvant effect and mechanism of anemoside B4 through network pharmacology and experiment verification, Phytomedicine 124 (2024 Feb) 155302.
[51] J. Liu, J. Cai, P. Fan, X. Dong, N. Zhang, J. Tai, Y. Cao, Salidroside alleviates dextran sulfate sodium-induced colitis in mice by modulating the gut microbiota, Food Funct. 14 (16) (2023 Aug 14) 7506–7519.
[52] H. Wu, Q. Rao, G.C. Ma, X.H. Yu, C.E. Zhang, Z.J. Ma, Effect of triptolide on dextran sodium sulfate-induced ulcerative colitis and gut microbiota in mice, Front. Pharmacol. 10 (2020 Jan 29) 1652.
[53] H. Guo, H. Guo, Y. Xie, Y. Chen, C. Lu, Z. Yang, Y. Zhu, Y. Ouyang, Y. Zhang, X. Wang, Mo3Se4 nanoparticle with ROS scavenging and multi-enzyme activity for the treatment of DSS-Induced colitis in mice, Redox Biol. 56 (2022 Oct) 102441.
[54] L. Chen, R.P. Vasoya, N.H. Toke, A. Parthasarathy, S. Luo, E. Chiles, J. Flores, N. Gao, E.M. Bonder, X. Su, M.P. Verzi, HNF4 regulates fatty acid oxidation and is required for renewal of intestinal stem cells in mice, Gastroenterology 158 (4) (2020 Mar) 985–999.e9.
[55] J. Liang, W. Dai, C. Liu, Y. Wen, C. Chen, Y. Xu, S. Huang, S. Hou, C. Li, Y. Chen, W. Wang, H. Tang, Gingerenone A attenuates ulcerative colitis via targeting IL-17RA to inhibit inflammation and restore intestinal barrier function, Adv. Sci. 11 (28) (2024 Jul) e2400206.
[56] H. Guo, H. Guo, Y. Xie, Y. Chen, C. Lu, Z. Yang, Y. Zhu, Y. Ouyang, Y. Zhang, X. Wang, Mo3Se4 nanoparticle with ROS scavenging and multi-enzyme activity for the treatment of DSS-Induced colitis in mice, Redox Biol. 56 (2022 Oct) 102441.
[57] L.C. Tong, Y. Wang, Z.B. Wang, W.Y. Liu, S. Sun, L. Li, D.F. Su, L.C. Zhang, Propionate ameliorates dextran sodium sulfate-induced colitis by improving intestinal barrier function and reducing inflammation and oxidative stress, Front. Pharmacol. 7 (2016 Aug 15) 253.
[58] D. Firoozi, S.J. Masoumi, S. Mohammad-Kazem Hosseini Asl, A. Labbe, I. Razeghian-Jahromi, M. Fararouei, K.B. Lankarani, M. Dara, Effects of short-chain fatty acid-butyrate supplementation on expression of circadian-clock genes, sleep quality, and inflammation in patients with active ulcerative colitis: a double-blind randomized controlled trial, Lipids Health Dis. 23 (1) (2024 Jul 13) 216.
[59] K.E. Bach Knudsen, H.N. Lærke, M.S. Hedemann, T.S. Nielsen, A.K. Ingerslev, D. S. Gundelund Nielsen, P.K. Theil, S. Purup, S. Hald, A.G. Schioldan, M.L. Marco, S. Gregersen, K. Hermansen, Impact of diet-modulated butyrate production on intestinal barrier function and inflammation, Nutrients 10 (10) (2018 Oct 13) 1499.
[60] G. Chen, X. Ran, B. Li, Y. Li, D. He, B. Huang, S. Fu, J. Liu, W. Wang, Sodium butyrate inhibits inflammation and maintains epithelium barrier integrity in a TNBS-Induced inflammatory bowel disease mice model, EBioMedicine 30 (2018 Apr) 317–325.
[61] G. Falony, A. Vlachou, K. Verbrugghe, L. De Vuyst, Cross-feeding between Bifidobacterium longum BB536 and acetate-converting, butyrate-producing Colon bacteria during growth on oligofructose, Appl. Environ. Microbiol. 72 (12) (2006 Dec) 7835–7841.
[62] P.F. de Groot, T. Nikolic, S. Imangaliyev, S. Bekkering, G. Duinkerken, F.M. Keij, H. Herrema, M. Winkelmeijer, J. Kroon, E. Levin, B. Hutten, E.M. Kemper, S. Simsek, J.H.M. Levels, F.A. van Hoorn, R. Bindraban, A. Berkvens, G. M. Dallinga-Thie, M. Davids, F. Holleman, J.B.L. Hoekstra, E.S.G. Stroes, M. Netea, D.H. van Raalte, B.O. Roep, M. Nieuwdorp, Oral butyrate does not affect innate immunity and islet autoimmunity in individuals with longstanding type 1 diabetes: a randomised controlled trial, Diabetologia 63 (3) (2020 Mar) 597–610.
[63] J. Xu, X. Chen, S. Yu, Y. Su, W. Zhu, Effects of early intervention with sodium butyrate on gut microbiota and the expression of inflammatory cytokines in neonatal piglets, PLoS One 11 (9) (2016 Sep 9) e0162461.